

---

# A Normative and Biologically Plausible Algorithm for Independent Component Analysis

---

Yanis Bahroun<sup>1,2</sup>    Dmitri B. Chklovskii<sup>1,4</sup>    Anirvan M. Sengupta<sup>2,3,5</sup>

<sup>1</sup> Center for Computational Neuroscience, Flatiron Institute

<sup>2</sup> Center for Computational Mathematics, Flatiron Institute

<sup>3</sup> Center for Computational Quantum Physics, Flatiron Institute

<sup>4</sup> Neuroscience Institute, NYU Medical Center

<sup>5</sup> Department of Physics and Astronomy, Rutgers University

{ybahroun,dchklovskii}@flatironinstitute.org anirvans.physics@gmail.com

## Abstract

The brain effortlessly solves blind source separation (BSS) problems, but the algorithm it uses remains elusive. In signal processing, linear BSS problems are often solved by Independent Component Analysis (ICA). To serve as a model of a biological circuit, the ICA neural network (NN) must satisfy at least the following requirements: 1. The algorithm must operate in the online setting where data samples are streamed one at a time, and the NN computes the sources on the fly without storing any significant fraction of the data in memory. 2. The synaptic weight update is local, i.e., it depends only on the biophysical variables present in the vicinity of a synapse. Here, we propose a novel objective function for ICA from which we derive a biologically plausible NN, including both the neural architecture and the synaptic learning rules. Interestingly, our algorithm relies on modulating synaptic plasticity by the total activity of the output neurons. In the brain, this could be accomplished by neuromodulators, extracellular calcium, local field potential, or nitric oxide.

## 1 Introduction

In the brain, visual, auditory, and olfactory systems effortlessly identify latent sources from their mixtures [1, 2, 3, 4]. In unsupervised learning, such task is known as blind source separation (BSS) [5]. BSS is often solved by Independent Component Analysis (ICA) [6, 7], which assumes a generative model, wherein the observed stimuli are linear combinations of independent sources. ICA algorithms determine the linear transformation back from the observed stimuli into their original sources without knowing how they were mixed in the first place.

Developing a biologically plausible ICA algorithm may provide critical insight into neural computational primitives because ICA may be implemented throughout the brain. In particular, receptive fields of V1 neurons may be the result of performing ICA on natural images [8, 9]. Similarly, ICA may account for the receptive fields in the auditory system [10]. Moreover, the neural computational primitives used in the visual and the auditory cortex may be similar, as evidenced by anatomical similarity and by developmental experiments where auditory cortex neurons acquire V1-like receptive fields when visual inputs are redirected there [11]. Therefore, ICA may serve as a computational primitive underlying learning throughout the neocortex.

The majority of existing ICA algorithms [5], for example, information-theoretic ones [12, 13, 14, 15, 16] do not meet our biological plausibility requirements. In this work, for the biological plausibility of neural networks (NN), we require that i) they operate in the online (or streaming) setting, namely, the input dataset is streamed one data vector at a time, and the corresponding output must be computed

without storing any significant fraction of the dataset in memory, ii) the weights of synapses in an NN must be updated using local learning rules, i.e., they depend only on the biophysical variables present in only the two neurons that the synapse connects or extracellular space near the synapse. Most existing bio-inspired ICA NNs [17, 18, 19, 20, 7] operate online but, when extracting multiple components, rely on non-local learning rules, i.e., a synapse needs to “know” about the individual activities of neurons other than the two it connects.

More biologically plausible ICA algorithms with local learning rules are limited to sources whose kurtosis deviates from the normal distribution in the same direction, are hand-crafted (ad hoc), and lack good theoretical guarantees [21, 22, 20]. An alternative to analyzing NNs with ad hoc learning rules is the normative approach. In the normative approach, an optimization problem with known offline solution is used as a starting point to derive online optimization algorithm which maps onto an NN with local learning rules. Such a normative approach led to the development of more biologically plausible ICA networks but only in limited settings of either nonnegative ICA [23, 24] or bounded component analysis [25, 26]

In this work, we develop a biologically plausible ICA neural network inspired by kurtosis-based ICA methods [27, 7, 28]. Specifically, we take inspiration in the Fourth-Order Blind Identification (FOBI) procedure which separates sources with distinct kurtosis [27]. In this context, distributions are often distinguished depending on their kurtosis relative to a Gaussian distribution, i.e., super- and sub-Gaussian distribution known respectively as leptokurtic (“spiky”) and platykurtic (“flat-topped”). Our normative approach is based on a novel similarity-preserving objective for ICA with an intuitive geometric interpretation. We reformulate this objective as a min-max optimization problem and solve it online by stochastic gradient optimization. We demonstrate that our algorithm performs well on synthetic datasets, audio signals, and natural images.

Our online algorithm maps onto a single-layer NN that can separate independent sources without pre-processing. The synaptic weights in our NN are updated using local learning rules, extending more conventional Hebbian learning rules by a time-varying modulating factor, which is a function of the total output activity. The presence of such a modulating factor suggests a role of the extracellular environment on synaptic plasticity. Modulation of the plasticity rules by overall output activity agrees with several experimental studies that have reported that a third factor, in addition to pre- and post-synaptic activities, can play a crucial role in modulating the outcome of Hebbian plasticity. This could be accomplished by neuromodulators [29, 30, 31, 32], extracellular calcium [33], local field potential [34], or nitric oxide [35, 36, 37].

## 2 Problem statement and inspiration

The problem of BSS consists of recovering a set of unobservable source signals from observed mixtures. When mixing is linear, BSS can be solved by ICA, which decomposes observed random vectors into statistically independent variables.

Mathematically, ICA assumes the following generative model. There are  $d$  sources recorded  $T$  times forming the columns of  $\mathbf{S} := [\mathbf{s}_1, \dots, \mathbf{s}_T] \in \mathbb{R}^{d \times T}$  whose components  $s_t^1, \dots, s_t^d$  are assumed non-Gaussian and independent. Without loss of generality, we assume that each source has zero-mean, unit variance, and finite kurtosis. We also assume that sources have distinct kurtosis as is commonly done in kurtosis-based ICA methods [28]. The kurtosis of a random variable  $v$  is defined as  $\text{kurt}[v] = \mathbb{E}[(v - \mathbb{E}(v))^4] / (\mathbb{E}[(v - \mathbb{E}(v))^2])^2$ . Finally, sources are linearly mixed, i.e., there exists a full rank mixing matrix,  $\mathbf{A} \in \mathbb{R}^{d \times d}$ , producing the  $d$ -dimensional mixture,  $\mathbf{x}_t$ :

$$\mathbf{x}_t = \mathbf{A}\mathbf{s}_t \quad \forall t \in \{1, \dots, T\} . \quad (1)$$

Then the goal of ICA algorithms is to determine a linear transformation of the observed signal,  $\mathbf{W}_{ICA} \in \mathbb{R}^{d \times d}$ , such that

$$\mathbf{y}_t := \mathbf{W}_{ICA}\mathbf{x}_t, \quad \forall t \in \{1, \dots, T\} , \quad (2)$$

recovers unknown sources possibly up to a permutation and a sign flip.

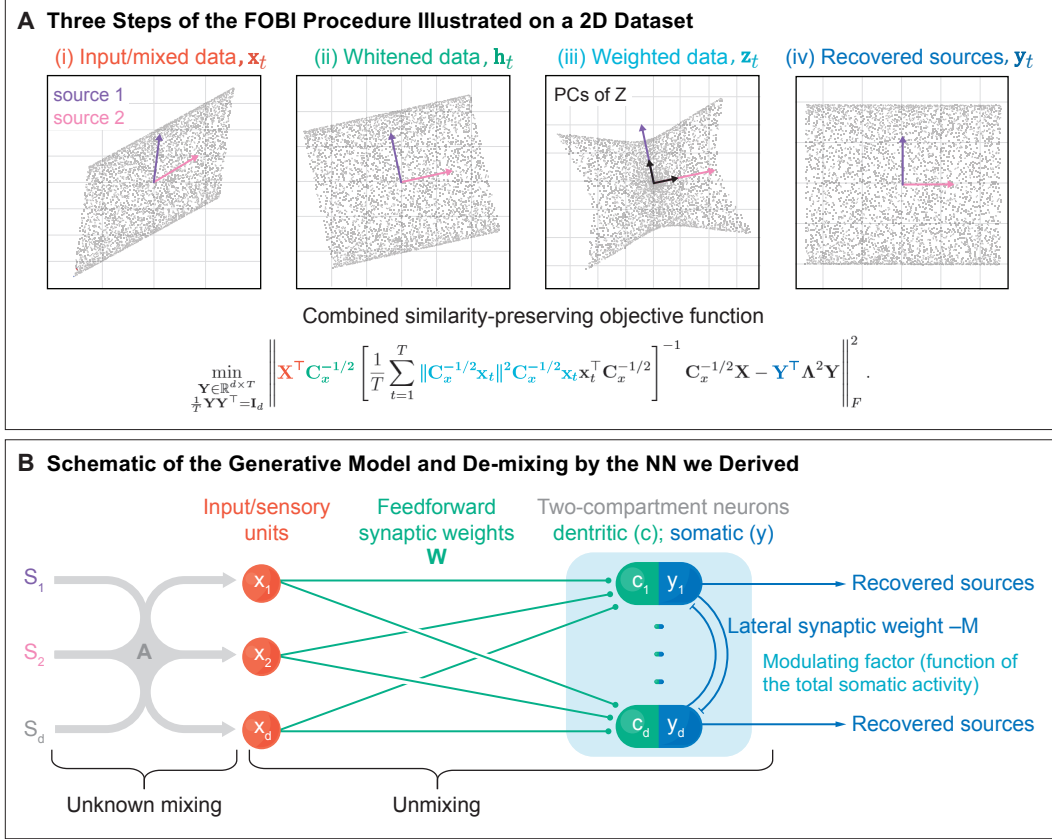


Figure 1: **A. The three steps of the FOBI procedure illustrated on a 2D dataset.** The purple and pink arrows show the axes of the independent sources  $s_i$ . **(i)** the observed signal,  $\mathbf{x}_t$ , **(ii)** the whitened data,  $\mathbf{h}_t$ , **(iii)** norm-weighted whitened data,  $\mathbf{z}_t$ , black arrows represent the principal directions of  $\mathbf{z}_t$  **(iv)** the recovered sources,  $\mathbf{y}_t$  are projections of  $\mathbf{h}_t$  onto the principal directions of  $\mathbf{z}_t$ . These three steps are combined into a single objective function as indicated by color-coding. **B. Schematic of the generative model and de-mixing by the NN we derived.** The output layer consists of two-compartment neurons whose synapses obey local learning rules. The dendritic compartments of the output neurons whiten data. The somatic compartments reconstruct the sources by rotating the whitened data. The pale blue rounded rectangle represents modulation of plasticity by output activity.

## 2.1 Review of the FOBI procedure

FOBI algorithm exploits a connection between ICA and Principal Component Analysis (PCA) [38, 39] pointed out in [27, 40]. We reproduce the proof of source recovery by FOBI from [27, 40] in Appendix A.

**Description of the procedure.** FOBI procedure consists of three steps, see **Fig. 1A**. First, the data must be whitened, i.e., all components become decorrelated and of unit variance, **Fig. 1A(ii)**. The whitening step can be performed using sample covariance,  $\mathbf{C}_x = \frac{1}{T} \sum_{t=1}^T \mathbf{x}_t \mathbf{x}_t^T$ , as follows:

$$\text{Step 1: whiten } \mathbf{h}_t = \mathbf{C}_x^{-1/2} \mathbf{x}_t .$$

Data whitening is often the first step in many ICA algorithms because recovering the sources after whitening corresponds to finding an orthogonal rotation matrix [17]. Various ICA methods differ in how the rotation is chosen. In FOBI, the whitened data,  $\mathbf{h}_t$ , is scaled by its norm and termed  $\mathbf{z}_t$ . Then, the directions of  $\mathbf{h}_t$  and  $\mathbf{s}_t$  with distinct kurtosis are recovered by finding the eigenvectors of

the sample covariance matrix  $\frac{1}{T} \sum_{t=1}^T \mathbf{z}_t \mathbf{z}_t^\top$ , **Fig. 1A(iii)**.

**Step 2a:** transform  $\mathbf{z}_t = \|\mathbf{h}_t\| \cdot \mathbf{h}_t$ ; **Step 2b:** optimize  $\mathbf{W}_z := \arg \max_{\substack{\mathbf{W} \in \mathbb{R}^{d \times d} \\ \mathbf{W}\mathbf{W}^\top = \mathbf{I}_d}} \frac{1}{T} \text{Tr} \left( \mathbf{W} \sum_{t=1}^T \mathbf{z}_t \mathbf{z}_t^\top \mathbf{W}^\top \right)$ .

Finally, to recover the sources, we project the whitened data,  $\mathbf{h}_t$ , onto the rows of  $\mathbf{W}_z$ , **Fig. 1A(iv)**

**Step 3:** project  $\mathbf{y}_t = \mathbf{W}_z \mathbf{h}_t$ .

**Can a biologically plausible NN implement the FOBI algorithm?** The first two steps of FOBI do not present a problem with a biological implementation. For example, **Step 2b**, essentially a PCA, can be solved by a stochastic gradient ascent algorithm using Oja’s learning rule [41]:

$$\Delta \mathbf{W}_z = \eta (\mathbf{u}_t \mathbf{z}_t^\top - \mathbf{u}_t \mathbf{u}_t^\top \mathbf{W}_z) . \quad (3)$$

Then, **Step 2b** can be mapped onto a single-layer network with upstream neurons’ activity encoding  $\mathbf{z}_t$ , and the output neurons computing the components of  $\mathbf{u}_t := \mathbf{W}_z \mathbf{z}_t$  where the elements of  $\mathbf{W}_z$  are encoded in the weights of feedforward synapses. Eq.(3) gives the weight update for the feedforward synapses with the learning rate,  $\eta > 0$ . However, according to **step 3**, the final output of FOBI must be  $\mathbf{y}_t$ , obtained by multiplying the whitened inputs,  $\mathbf{h}_t$ , by  $\mathbf{W}_z$  without scaling them by their norm. Such output may be computed by another single-layer network with the same feedforward synaptic weights,  $\mathbf{W}_z$ , but that would require weight-sharing (or weight transport). Alternatively, avoiding weight transport would require a non-local update rule for  $\mathbf{W}_z$ . Thus, both alternatives lead to biologically implausible solutions.

## 2.2 Similarity matching for principal subspace analysis

To find a biologically plausible implementation of FOBI, we follow the approach used previously to derive biologically plausible networks for Principal Subspace Projection (PSP) [42], a variant of PCA, and other tasks[43, 44, 45, 46, 47, 48, 49, 50, 51, 52, 53, 54]. This approach starts from reformulating the optimization objective for PSP in the so-called Similarity Matching (SM) form [55]:

$$\min_{\mathbf{Y} \in \mathbb{R}^{m \times T}} \|\mathbf{X}^\top \mathbf{X} - \mathbf{Y}^\top \mathbf{Y}\|_F^2 , \quad (4)$$

where  $\mathbf{X} := [\mathbf{x}_1, \dots, \mathbf{x}_T]$  is the data matrix,  $\mathbf{Y} := [\mathbf{y}_1, \dots, \mathbf{y}_T]$  is the output matrix, and  $\|\cdot\|_F$  the Frobenius norm. In turn, the objective (4) can be optimized by an online algorithm that maps onto a single-layer network of linear neurons whose synapses obey local learning rules [44].

Whereas the SM approach leads to biologically plausible NNs for solving eigenproblems, it was still unclear how to overcome the weight transport challenge arising in the FOBI algorithm implementation. In the next Section, we address this challenge by introducing a novel SM objective for ICA.

## 3 A similarity-preserving objective for ICA

To derive a single-layer NN for ICA, which can be trained with local learning rules, we adopt a normative approach. We design a novel objective function, the solution of which projects the whitened data,  $\mathbf{h}_t$ , onto the eigenvectors of the covariance of  $\mathbf{z}_t$  as specified in the FOBI procedure above using the SM approach. Specifically, we propose the following generalized nonlinearly weighted similarity matching objective using the notations,  $\mathbf{H} := [\mathbf{h}_1, \dots, \mathbf{h}_T]$  and  $\mathbf{Z} := [\mathbf{z}_1, \dots, \mathbf{z}_T]$  as defined earlier in Sec. 2.1 and illustrated in **Fig. 1A**,

$$\min_{\mathbf{Y} \in \mathbb{R}^{d \times T}} \left\| \mathbf{H}^\top \left[ \frac{1}{T} \mathbf{Z} \mathbf{Z}^\top \right]^{-1} \mathbf{H} - \mathbf{Y}^\top \mathbf{\Lambda}^2 \mathbf{Y} \right\|_F^2 , \quad \text{s.t.} \quad \frac{1}{T} \mathbf{Y} \mathbf{Y}^\top = \mathbf{I}_d , \quad (5)$$

with  $\mathbf{\Lambda}^2 = \text{diag}(\lambda_1^2, \dots, \lambda_d^2)$  any diagonal matrix with distinct finite positive entries.

To accomplish all the three steps above in a single-layer network, we rewrite (5) in terms of the input data  $\mathbf{X}$  by substituting the expressions for  $\mathbf{H}$  (**Step 1**) and  $\mathbf{Z}$  (**Step 2a**):

$$\min_{\substack{\mathbf{Y} \in \mathbb{R}^{d \times T} \\ \frac{1}{T} \mathbf{Y} \mathbf{Y}^\top = \mathbf{I}_d}} \left\| \mathbf{X}^\top \mathbf{C}_x^{-1/2} \left[ \frac{1}{T} \sum_{t=1}^T \|\mathbf{C}_x^{-1/2} \mathbf{x}_t\|^2 \mathbf{C}_x^{-1/2} \mathbf{x}_t \mathbf{x}_t^\top \mathbf{C}_x^{-1/2} \right]^{-1} \mathbf{C}_x^{-1/2} \mathbf{X} - \mathbf{Y}^\top \mathbf{\Lambda}^2 \mathbf{Y} \right\|_F^2 . \quad (6)$$

Then the global minima of objective (6) recover the sources as formalized by the following theorem:

**Theorem 1.** *Given that the sources are independent, centered, have unit variance, and distinct kurtosis (c.f. Sec 2), then the global optimal solution for our objective (6), denoted by  $\mathbf{Y}^*$  satisfies*

$$\mathbf{Y}^* = \mathbf{\Xi} \mathbf{\Pi} \mathbf{S} \quad (7)$$

where  $\mathbf{\Xi}$  is a diagonal matrix with  $\pm 1$ 's on the diagonal, and  $\mathbf{\Pi}$  is a permutation matrix, and is thus a solution to the ICA problem.

*Proof.* We give the detailed proof of the theorem in Appendix A.  $\square$

## 4 Derivation of the algorithm

While our objective (6) can be minimized by taking gradient descent steps with respect to  $\mathbf{Y}$ , this would not lead to an online algorithm because such computation requires combining data from different time steps. Instead, following [44], we introduce auxiliary matrix variables corresponding to synaptic weights, which store sufficient statistics allowing for the ICA computation using solely instantaneous inputs. Such substitution leads to a min-max optimization problem that is solved by gradient descent/ascent. A corresponding online optimization algorithm using stochastic gradient descent/ascent maps onto an NN with local learning rules.

### 4.1 Min-max formulation

Here we modify the objective (6) by introducing auxiliary variables, namely  $\mathbf{W}$  and  $\mathbf{M}$ , leading to a min-max optimization problem. In the following sub-sections, the gradient descent/ascent optimization of the min-max objective will lead to an online algorithm that maps onto an NN where  $\mathbf{W}$  and  $\mathbf{M}$  correspond to synaptic weights.

We expand the square in Eq. (6), normalizing by  $T^2$ , and dropping terms that do not depend on  $\mathbf{Y}$  yielding:

$$\min_{\mathbf{Y} \in \mathbb{R}^{d \times T}} \frac{1}{T^2} \text{Tr} \left( -2\mathbf{X}^\top \mathbf{\Gamma}_x \mathbf{X} \mathbf{Y}^\top \mathbf{\Lambda}^2 \mathbf{Y} + \mathbf{Y}^\top \mathbf{\Lambda}^2 \mathbf{Y} \mathbf{Y}^\top \mathbf{\Lambda}^2 \mathbf{Y} \right) \quad \text{s.t.} \quad \frac{1}{T} \mathbf{Y} \mathbf{Y}^\top = \mathbf{I}_d, \quad (8)$$

where, for convenience, we introduce

$$\mathbf{\Gamma}_x := \mathbf{C}_x^{-1/2} \left[ \frac{1}{T} \sum_{t=1}^T \|\mathbf{C}_x^{-1/2} \mathbf{x}_t\|^2 \mathbf{C}_x^{-1/2} \mathbf{x}_t \mathbf{x}_t^\top \mathbf{C}_x^{-1/2} \right]^{-1} \mathbf{C}_x^{-1/2}.$$

The quartic term in  $\mathbf{Y}$  in (8) is a constant under the decorrelation constraint and can be dropped from the optimization.

We now introduce auxiliary matrix variables  $\mathbf{W}$  and  $\mathbf{M}$ , resulting in:

$$\min_{\mathbf{Y} \in \mathbb{R}^{d \times T}} \min_{\mathbf{W} \in \mathbb{R}^{d \times d}} \max_{\mathbf{M} \in \mathbb{R}^{d \times d}} \mathcal{L}(\mathbf{W}, \mathbf{M}, \mathbf{Y}), \quad (9)$$

where  $\mathcal{L}(\mathbf{W}, \mathbf{M}, \mathbf{Y}) := \frac{1}{T} \text{Tr} \left( -2\mathbf{X}^\top \mathbf{W}^\top \mathbf{Y} + \mathbf{Y}^\top \mathbf{M} \mathbf{Y} \right) + \text{Tr} \left( \mathbf{W} \mathbf{\Gamma}_x^{-1} \mathbf{W}^\top \mathbf{\Lambda}^{-2} - \mathbf{M} \right).$

To verify the equivalence between the minimization problem (8) and the min-max problem (9) take partial derivatives of  $\mathcal{L}(\mathbf{W}, \mathbf{M}, \mathbf{Y})$  with respect to  $\mathbf{W}$  (resp.  $\mathbf{M}$ ) and note that the minimum (resp. maximum) is achieved when  $\mathbf{W} = \frac{1}{T} \mathbf{\Lambda}^2 \mathbf{Y} \mathbf{X}^\top \mathbf{\Gamma}_x$  (resp.  $\frac{1}{T} \mathbf{Y} \mathbf{Y}^\top = \mathbf{I}_d$ ). Substituting optimal  $\mathbf{W}$  and  $\mathbf{M}$  leads back to (8).

Finally, interchanging the order of minimization with respect to  $\mathbf{Y}$ , with the optimization with respect to  $\mathbf{W}$  and  $\mathbf{M}$ , yields

$$\min_{\mathbf{W} \in \mathbb{R}^{d \times d}} \max_{\mathbf{M} \in \mathbb{R}^{d \times d}} \min_{\mathbf{Y} \in \mathbb{R}^{d \times T}} \mathcal{L}(\mathbf{W}, \mathbf{M}, \mathbf{Y}). \quad (10)$$

The interchange is justified by saddle point property of  $\mathcal{L}(\mathbf{W}, \mathbf{M}, \mathbf{Y})$  with respect to  $\mathbf{Y}$  and  $\mathbf{M}$  [44].

## 4.2 Gradient optimization in the offline setting

In this subsection, we optimize the objective (6) in the offline setting, where the entire data matrix  $\mathbf{X}$  is accessible. In this case, we solve the min-max problem (9) by alternating optimization steps. For fixed  $\mathbf{W}$  and  $\mathbf{M}$ , we minimize the objective function  $\mathcal{L}(\mathbf{W}, \mathbf{M}, \mathbf{Y})$  over  $\mathbf{Y}$ , which yields the relation

$$\mathbf{Y} := \arg \min_{\mathbf{Y} \in \mathbb{R}^{d \times T}} \mathcal{L}(\mathbf{W}, \mathbf{M}, \mathbf{Y}) = \mathbf{M}^{-1} \mathbf{W} \mathbf{X} . \quad (11)$$

Before applying gradient optimization steps of the objective function  $\mathcal{L}(\mathbf{W}, \mathbf{M}, \mathbf{Y})$  with respect to  $\mathbf{W}$  and  $\mathbf{M}$ , we first simplify  $\mathbf{\Gamma}_x^{-1}$  appearing in (10), as a part of the term,  $\text{Tr}(\mathbf{W} \mathbf{\Gamma}_x^{-1} \mathbf{W}^\top \mathbf{\Lambda}^{-2})$ ,

$$\mathbf{\Gamma}_x^{-1} = \mathbf{C}_x^{1/2} \left[ \frac{1}{T} \sum_{t=1}^T \|\mathbf{C}_x^{-1/2} \mathbf{x}_t\|^2 \mathbf{C}_x^{-1/2} \mathbf{x}_t \mathbf{x}_t^\top \mathbf{C}_x^{-1/2} \right] \mathbf{C}_x^{1/2} = \frac{1}{T} \sum_t \alpha_t \mathbf{x}_t \mathbf{x}_t^\top , \quad (12)$$

where  $\alpha_t = \|\mathbf{C}_x^{-1/2} \mathbf{x}_t\|^2$  is the squared norm of the whitened data. As the transformation from whitened data to the recovered sources is an orthogonal rotation, the squared norm of the sources and of the outputs is preserved:

$$\alpha_t = \|\mathbf{C}_x^{-1/2} \mathbf{x}_t\|^2 = \|\mathbf{s}_t\|^2 = \|\mathbf{y}_t\|^2 . \quad (13)$$

We then use (13) to rewrite (12) as

$$\mathbf{\Gamma}_x^{-1} = \frac{1}{T} \mathbf{X} \text{ddiag}(\mathbf{Y}^\top \mathbf{Y}) \mathbf{X}^\top = \frac{1}{T} \sum_{t=1}^T \|\mathbf{y}_t\|^2 \mathbf{x}_t \mathbf{x}_t^\top , \quad (14)$$

where  $\text{ddiag}(\cdot)$  represents a diagonal matrix which keeps only the diagonal elements of the argument matrix.

We now obtain the update rules for  $\mathbf{W}$  and  $\mathbf{M}$  by gradient-descent ascent on (10) and by replacing  $\mathbf{\Gamma}_x^{-1}$  according to (14)

$$\mathbf{W} \leftarrow \mathbf{W} + 2\eta \left( \frac{1}{T} \mathbf{Y} \mathbf{X}^\top - \mathbf{\Lambda}^{-2} \mathbf{W} \mathbf{\Gamma}_x^{-1} \right) = \mathbf{W} + \frac{2\eta}{T} \left( \mathbf{Y} \mathbf{X}^\top - \mathbf{\Lambda}^{-2} \mathbf{W} \mathbf{X} \text{ddiag}(\mathbf{Y}^\top \mathbf{Y}) \mathbf{X}^\top \right) , \quad (15)$$

$$\mathbf{M} \leftarrow \mathbf{M} + \frac{\eta}{\tau} \left( \frac{1}{T} \mathbf{Y} \mathbf{Y}^\top - \mathbf{I}_d \right) . \quad (16)$$

Here  $\tau > 0$  is the ratio between the learning rates for  $\mathbf{W}$  and  $\mathbf{M}$ , and  $\eta \in (0, \tau)$  is the learning rate for  $\mathbf{W}$ , ensuring that  $\mathbf{M}$  remains positive definite given a positive definite initialization.

## 4.3 Online algorithm

We now solve the min-max objective (9) in the online setting. At each time step,  $t$ , we minimize over the output,  $\mathbf{y}_t$ , by repeating the following gradient descent steps until convergence:

$$\mathbf{y}_t \leftarrow \mathbf{y}_t + \gamma (\mathbf{c}_t - \mathbf{M} \mathbf{y}_t) , \quad (17)$$

where  $\gamma$  is a small step size, and we have defined the projection  $\mathbf{c}_t := \mathbf{W} \mathbf{x}_t$ , with biological interpretation described in Sec 5. As in (11), the dynamics converge to  $\mathbf{y}_t = \mathbf{M}^{-1} \mathbf{c}_t$ . We now take stochastic gradient descent-ascent steps in  $\mathbf{W}$  and  $\mathbf{M}$ . We thus replace the averages in Eqs. (15)-(16) with their online approximations

$$\frac{1}{T} \mathbf{Y} \mathbf{X}^\top \rightarrow \mathbf{y}_t \mathbf{x}_t^\top ; \quad \frac{1}{T} \mathbf{Y} \mathbf{Y}^\top \rightarrow \mathbf{y}_t \mathbf{y}_t^\top ; \quad \frac{1}{T} \mathbf{\Lambda}^{-2} \mathbf{W} \mathbf{X} \text{ddiag}(\mathbf{Y}^\top \mathbf{Y}) \mathbf{X}^\top \rightarrow \|\mathbf{y}_t\|^2 \mathbf{\Lambda}^{-2} \mathbf{c}_t \mathbf{x}_t^\top .$$

This yields our online ICA algorithm (Algorithm 1) and the NN, see Section 5.

## 5 Biological interpretation and neural implementation

We now show that our online ICA algorithm (Algorithm 1) maps onto an NN with local, activity-dependent synaptic update rules, which emulate aspects of synaptic plasticity observed experimentally.

---

**Algorithm 1** A similarity-preserving algorithm for Independent Component Analysis.

---

**input** data  $\{\mathbf{x}_1, \dots, \mathbf{x}_T\}$ ; dimension  $d$   
**output**  $\{\mathbf{y}_1, \dots, \mathbf{y}_T\}$ ; dimension  $d$  ▷ estimated sources  
**initialize** the matrix  $\mathbf{W}$ , and positive definite matrix  $\mathbf{M}$ .  
**for**  $t = 1, 2, \dots, T$  **do**  
     $\mathbf{c}_t \leftarrow \mathbf{W}\mathbf{x}_t$  ; ▷ projection of inputs  
    **run the following until convergence:**  
         $\frac{d\mathbf{y}_t(\gamma)}{d\gamma} = \mathbf{c}_t - \mathbf{M}\mathbf{y}_t(\gamma)$  ; ▷ neural dynamics  
         $\mathbf{W} \leftarrow \mathbf{W} + 2\eta(\mathbf{y}_t - \|\mathbf{y}_t\|^2\mathbf{\Lambda}^{-2}\mathbf{c}_t)\mathbf{x}_t^\top$  ;  $\mathbf{M} \leftarrow \mathbf{M} + \frac{\eta}{\tau}(\mathbf{y}_t\mathbf{y}_t^\top - \mathbf{I}_d)$  ; ▷ synaptic updates  
    **end for**

---

## 5.1 Neural architecture and dynamics

Our algorithm can be implemented by a biologically plausible NN presented in **Fig. 1B**. The network consists of an input layer of  $d$  neurons, representing the input data to be separated into independent components, and an output layer of  $d$  neurons, with separate dendritic and somatic compartments, estimating the unknown sources. The network includes a set of feedforward synapses between the inputs and the dendrites of the output neurons as well as a set of lateral synapses between the output somas **Fig. 1B**.

Although two-compartment neurons have not been common in machine learning, in neuroscience, they are often used to model pyramidal cells - the most numerous neuron type in the neocortex. Such neuron consists of an apical dendritic compartment, as well as a somatic compartment, which have distinct membrane potentials [56, 57, 58, 59]. Recently, such two-compartment neurons appeared in bio-inspired machine learning algorithms [60, 61, 62, 51, 63, 64].

At each time step  $t$ , the network computes in two phases. First, the mixture  $\mathbf{x}_t$ , represented in the input neurons, is multiplied by the weight matrix  $\mathbf{W}$  encoded by the feedforward synapses connecting the input neurons to the output neurons. This yields the projection  $\mathbf{c}_t = \mathbf{W}\mathbf{x}_t$  computed in the dendritic compartments of the output neurons and then propagated to their somatic compartments.

Second, the  $d$ -dimensional output signal  $\mathbf{y}_t$  is computed as somatic activity in the output neurons and corresponds to the estimated sources. This is accomplished by the fast recurrent neural dynamics in lateral connection, Eq. (17), converging to the equilibrium value assignment of  $\mathbf{y}_t$  in Algorithm 1. The lateral synapses in **Fig. 1B** implement only the off-diagonal elements of  $\mathbf{M}$ . Whereas diagonal elements of  $\mathbf{M}$  would correspond to autapses (self-coupling of neurons), such Hebbian/anti-Hebbian networks can be designed without them [44, 45].

## 5.2 Synaptic plasticity rules

To highlight the locality of our learning rules, we rewrite the element-wise synaptic updates for  $\mathbf{W}$  and  $\mathbf{M}$  in Algorithm 1 using sub-/super-scripts:

$$W_{ij} \leftarrow W_{ij} + 2\eta \left( y_t^i x_t^j - \|\mathbf{y}_t\|^2 \frac{c_t^i}{\lambda_i^2} x_t^j \right) ; M_{ij} \leftarrow M_{ij} + \frac{\eta}{\tau} \left( y_t^i y_t^j - \delta_{ij} \right), 1 \leq i, j \leq d. \quad (18)$$

In Eqs. (18),  $x_t^j$  is the activity of the  $j^{th}$  input neuron,  $y_t^i$  is the activity of the  $i^{th}$  output neuron, and  $c_t^j$  is the dendritic current of the  $j^{th}$  output neuron, all at time  $t$ . Furthermore, the influence of the dendritic current  $c_t^j$  on a synapse's strength is modulated by the term  $\|\mathbf{y}_t\|^2$ , representing the overall activity of the output neurons.

How could total output neuronal activity be signaled to each feedforward synapse in the network? There are several diffusible molecules in the brain which may affect synaptic plasticity and whose concentration may depend on the overall neural activity. These include extracellular calcium [33], GABA[29, 65], dopamine [30, 66, 67], noradrenaline [31, 68], D-Serin [32, 69, 70] or nitric oxide (NO), although its range of action is contested [35, 36, 37]. Finally, local field potential can also affect synaptic plasticity [34]. For the learning rule to function in the online setting signaling must be fast, a requirement favoring local field potential and extracellular calcium out of the above candidates.

The learning rule (18) for feedforward synaptic weights,  $\mathbf{W}$ , simplifies significantly near the optimum of the objective,  $\mathbf{M} \approx \mathbf{I}_d$ , and for the converged output activity,  $\mathbf{c}_t = \mathbf{W}\mathbf{x}_t = \mathbf{M}\mathbf{y}_t$ :

$$\Delta \mathbf{W} = \eta_t (\mathbf{I} - \|\mathbf{y}_t\|^2 \Lambda^{-2} \mathbf{M}) \mathbf{y}_t \mathbf{x}_t^\top \approx \eta_t (\mathbf{I} - \|\mathbf{y}_t\|^2 \Lambda^{-2}) \mathbf{y}_t \mathbf{x}_t^\top . \quad (19)$$

Such an update is a nonlinearly modulated Hebbian learning rule where the sign of plasticity changes with the total output activity. For low total output activity,  $\|\mathbf{y}_t\|^2 < \lambda_i^2$ , the update is Hebbian, i.e., long-term potentiation (LTP) for correlated inputs and outputs. For high output activity,  $\|\mathbf{y}_t\|^2 > \lambda_i^2$ , the update is anti-Hebbian, i.e., long-term depression (LTD) for correlated inputs and outputs. We compare and contrast this global activity-dependent modulation of plasticity with the Bienenstock, Cooper, and Munro (BCM) rule in subsection 5.3.

Whereas three-factor learning has been invoked in multiple computational, especially reward-based, models [71, 72, 73, 74], our model is the first to propose such learning in the fully normative approach for ICA.

### 5.3 Comparison with existing rules

To understand the distinctive features of our model versus existing approaches, we compare and contrast it with three existing models: 1. Oja’s learning rule, 2. BCM learning rule [75], and 3. error-gated Hebbian rule (EGHR) [69].

**1. Nonlinear Oja’s learning rule.** [76, 19] generalized the original Oja’s rule, Eq. (3), with a component-wise nonlinear function  $g(\cdot)$  as  $\Delta \mathbf{W} = g(\mathbf{y}_t) \mathbf{x}_t^\top - g(\mathbf{y}_t) g(\mathbf{y}_t)^\top \mathbf{W}$ . However, this model and follow-up work inherited the main drawbacks of the standard Oja’s rule, i.e., they require pre-whitening of the data and rely on non-local learning rules. Indeed, the last term of the learning rules of nonlinear Oja implies that updating the weight of a synapse requires precise knowledge of output activities of all other neurons which are not available to the synapse (cf. [77] for details on standard PCA rules and networks of nonlinear neurons [78]).

**2. BCM learning rule.** Switching of the sign of plasticity depending on the total output activity Eq. (19) is reminiscent of the BCM rule. It was initially postulated and later connected to an objective function [79, 80] characterizing the deviation from Gaussian distribution but mainly focusing on skewness rather than kurtosis as in our model. For correlated input and output, the BCM rule induces LTD for “sub-threshold” responses and LTP for “super-threshold” responses, with the threshold being a function of average output activity. Unfortunately, multiple output BCM neurons respond to the same dominant feature, producing an incomplete, highly redundant code [79, 80]. In contrast, our network has lateral inhibitory connections whose weights are updated via anti-Hebbian rule Eq. (18) leading to the recovery of multiple sources. Although experimental evidence has validated BCM-like plasticity in parts of the visual cortex and the hippocampus, other brain areas have yet to show similar behavior. Interestingly, an “inverse” BCM rule, similar to ours has been proposed in the cerebellum [81, 82, 83].

**3. Modulated Hebbian rules.** Recent neural implementations of ICA [69, 74, 70] also introduced modulated Hebbian rules:  $\Delta \mathbf{W} = (E_0 - E(\mathbf{y}_t)) g(\mathbf{y}_t) \mathbf{x}_t^\top$ , with  $E_0$  a constant,  $E(\cdot)$  a nonlinear function of the total activity, and  $g(\cdot)$  a component-wise nonlinear function. This learning rule shares many similarities with ours. The term  $E_0$  is a constant characterizing the source distributions, which could identify with our  $\lambda_i$  terms, and the function  $E(\cdot)$  resembles our  $\|\mathbf{y}_t\|^2$  but is model dependent in their approach. This is where the similarities end as their objective function is inspired by the information-theoretic framework [12, 7] and ours - by the insight from the FOBI procedure [27, 84] and spectral methods from the SM method [44].

Their model can be considered partly normative since the neural architecture is predetermined and uses a hand-designed error-computing neuron to determine the global modulating factor rather than having been derived from an optimization problem. Interestingly, their model does not use lateral connections for output decorrelation resulting in a model without direct interaction between outputs. The presence of pairwise inhibitory interaction is crucial for our algorithm, leading to a globally optimal solution when the sources have distinct kurtosis. Numerical and theoretical analysis of the performance of the EGHR algorithm relies on the source distributions being the same and resulting in several equivalent optima.



## 6 Numerical simulations

In this section, we verify our theoretical results in numerical experiments. We use our model to perform ICA on both synthetic and real-world datasets. We designed three sets of experiments to illustrate the performance of our algorithm. In the first set, **Fig. 2A**, we used as sources artificially generated signals, in the second - natural speech signals, **Fig. 2B**, and in the third - natural scene images, **Fig. 2C**. According to the generative model, Eq. (1), we then used random full rank square mixing matrices,  $\mathbf{A}$ , to generate the observed mixed signals,  $\mathbf{x}_t$ . From  $\mathbf{x}_t$ , we aimed to recover the original sources. We show that our algorithm recovers sources regardless of sub- or super-Gaussianity of the kurtosis, which is essential for natural datasets. For details on the parameters used, see Appendix C.

**Synthetic data.** We first evaluate our algorithm on a synthetic dataset generated by independent and identically distributed samples. The data are generated from periodic signals, i.e., square-periodic, sine-wave, saw-tooth, and Laplace random noise. The data were chosen with the purpose of including both super- and sub-Gaussian distribution known respectively as leptokurtic (“spiky”, e.g., the Laplace distribution) and platykurtic (“flat-topped”, the three other source signal). We show in **Fig. 2A** the mixed signals in black, on the left plots. We show on the right plot the recovered sources, in red, overlapped with the original sources, in blue, and the residual in green. We also show the histogram of each signal on the right side of each plot. Results are shown for 300 samples. We observe that the recovered and true sources nearly perfectly overlap, explaining the low value of the residual, which shows the almost perfect reconstruct performed by our algorithm.

In Appendix **D**, we provide a numerical comparison of the performance of our algorithm with competing models, namely, Herault-Jutten algorithm [85], EASI algorithm [86, 87], Bell and Sejnowski’s algorithm [12], the Amari algorithm [13], and finally nonlinear Oja algorithm [88, 76]. These models were designed with NNs in mind and are seminal works on neural ICA algorithms. However, like nonlinear Oja algorithm, which is mentioned in Section 5.3.1, these models suffer from biological implausibility. In brief, our model either outperforms or is competitive with the models mentioned above. These results also confirm that our algorithm can deal with combinations of sub- and super-Gaussian sources, with or without pre-whitening of the data.

**Real-world data: Speech signals.** For the audio separation task, we used speech recordings from the freely available TSP data set [89]<sup>1</sup>, recorded at 16kHz. The first source we use was obtained from a male speaker (MA02 04.wav), the second source from a female speaker (FA01 03.wav), and the third source synthetically generated from a uniform noise, as was previously used in the literature [90]. We show our results in **Fig. 2B**. We show the mixtures, the true sources, the recovered sources, and the residual. It is clear from the figure that our algorithm’s outputs recover the true sources similarly to the synthetic dataset.

**Real-world data: Natural scene images.** We finally applied our algorithm to the task of recovering images from their mixtures, on data already used for BSS tasks [7, 91, 23]<sup>2</sup>, as shown in **Fig. 2C**. Here, we show separately the original sources, top images, the mixtures, middle images, and the recovered sources, bottom images of **Fig. 2C**. We considered three grayscale images of size  $256 \times 512$  pixels (shifted and scaled to have zero-mean and unit variance), such that each image is treated as one source, with the pixel intensities representing the samples. We again observe in **Fig. 2C** that the recovered sources are nearly identical to the original sources. We can also see that the histograms of the recovered sources nearly match the histograms of the original sources, up to their sign.

## 7 Discussion

We proposed a new single-layer ICA NN with biologically plausible local learning rules. The normative nature of our approach makes the biologically realistic features of our NNs readily interpretable. In particular, our NN uses neurons with two separate compartments and is trained with extended Hebbian learning rules. The changes in synaptic strength are modulated by the total output neuronal activity, equivalent to performing gradient optimization of our objective function. We demonstrated that the proposed rule reliably converges to the correct solution over a wide range of mixing matrices, synthetic, and natural datasets. The broad applicability and easy implementation

<sup>1</sup>Freely available at <http://www.mmsp.ece.mcgill.ca/Documents/Data/> (Accessed May 24th 2021).

<sup>2</sup>Freely available at <https://research.ics.aalto.fi/ica/data/images/> (Accessed May 24th 2021).

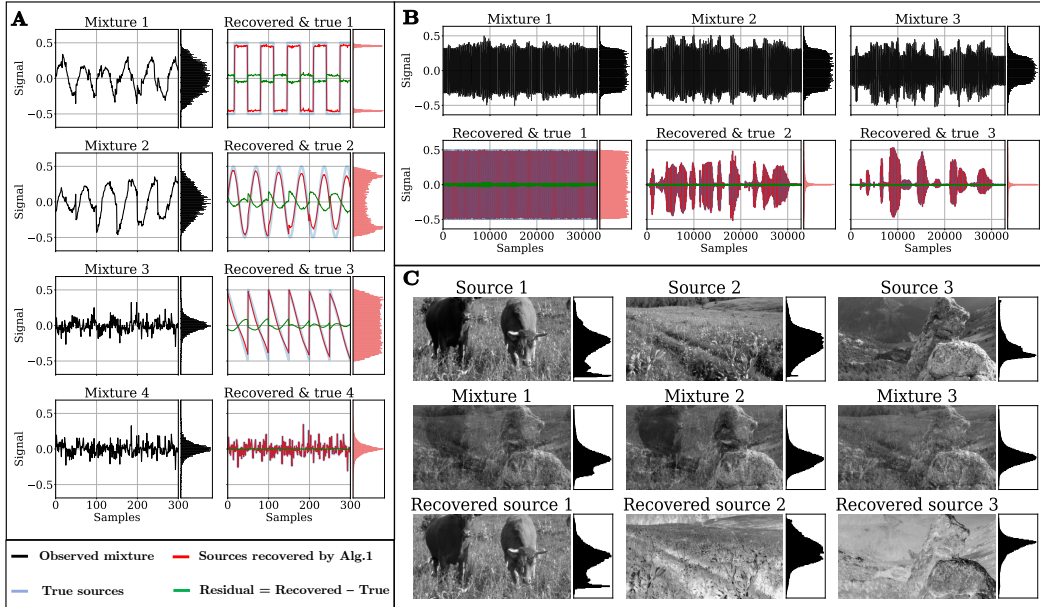


Figure 2: **Our ICA algorithm recovers independent sources from synthetic and real-world mixtures.** **A.** Synthetic data, **B.** Natural speech data, **C.** Natural image data. In **A-B.** mixed signals are shown in black, the recovered signals - in red, the true sources - in blue, and their residual difference - in blue. We also show the associated distributions. **C.** The sources, mixture, and recovered sources, in top, middle and bottom rows respectively.

of our NN and learning rules could further advance neuromorphic computation [92, 93, 94] and may reveal the principle underlying BSS computation in the brain.

Recent work on canonical correlation analysis [95, 96, 97], slow feature analysis [98], and ICA-like algorithms have led to biologically plausible NNs [99, 100, 101, 102], some of which rely on two-compartment neurons [103, 51]. These NNs could, in principle, be used for popular BSS tasks known as second-order blind identification [104, 105, 106, 107] or in the context of kernel ICA [108, 109]. This suggests the existence of a single model of two-compartment neurons and non-trivial local learning rules for BS. In future work, we aim at proposing such a model, including high-order statistics, temporal correlation, and diversity of views.

One limitation of our approach is the inability of the model to separate sources with the same kurtosis. Yet, as long as sources possess some distinct even-order moments, our scaling rule can be altered to separate the sources [27]. Another limitation is the well-known sensitivity of kurtosis to outliers. This limitation could be overcome if scaling varies as a sublinear function of the total activity [40]. These changes do not affect the neural architecture nor the locality of the learning rules.

Clarifying the limitations of our model leads us to ask various follow-up questions left for future work. How can we further generalize the solution beyond the choice of nonlinearity and beyond the task of linear ICA? We could envision considering more than two covariance matrices as in the JADE algorithm [110, 111, 112], which effectively performs joint-diagonalization of arbitrarily many matrices. A neural solution was proposed in [113] but again relies on non-local Oja-based rules. Ongoing work on nonlinear ICA [114, 115] is of great interest to us since it might be a perfect candidate for multi-layered architectures.

Recently, several works proposed biologically plausible supervised learning algorithms [61, 62, 63, 53, 116]. Combining these with ICA and unsupervised learning algorithms in general would provide a more comprehensive description of cognitive processes.

## Acknowledgments and Disclosure of Funding

Y.B. is grateful to Romain Cosentino, and Claudia Skok Gibbs for insightful discussions related to this work and feedback on this manuscript. We also thank the members of the Neural Circuits and Algorithms Group at the Flatiron Institute for providing feedback on an early version of this work.

The authors did not receive any third party funding for the completion of this project.

## References

- [1] Robert Desimone and John Duncan. Neural mechanisms of selective visual attention. *Annual Review of Neuroscience*, 18(1):193–222, 1995.
- [2] Rachel I Wilson and Zachary F Mainen. Early events in olfactory processing. *Annual Review of Neuroscience*, 29:163–201, 2006.
- [3] Mark A Bee and Christophe Micheyl. The cocktail party problem: what is it? how can it be solved? and why should animal behaviorists study it? *Journal of comparative psychology*, 122(3):235, 2008.
- [4] Josh H McDermott. The cocktail party problem. *Current Biology*, 19(22):R1024–R1027, 2009.
- [5] Pierre Comon and Christian Jutten. *Handbook of Blind Source Separation: Independent component analysis and applications*. Academic press, 2010.
- [6] Pierre Comon. Independent component analysis, a new concept? *Signal processing*, 36(3):287–314, 1994.
- [7] Aapo Hyvärinen and Erkki Oja. Independent component analysis: algorithms and applications. *Neural Networks*, 13(4-5):411–430, 2000.
- [8] Anthony Bell and Terrence J Sejnowski. Edges are the ‘independent components’ of natural scenes. *Advances in Neural Information Processing Systems*, 9:831–837, 1996.
- [9] Anthony J Bell and Terrence J Sejnowski. The “independent components” of natural scenes are edge filters. *Vision research*, 37(23):3327–3338, 1997.
- [10] Michael S Lewicki. Efficient coding of natural sounds. *Nature neuroscience*, 5(4):356–363, 2002.
- [11] Jitendra Sharma, Alessandra Angelucci, and Mriganka Sur. Induction of visual orientation modules in auditory cortex. *Nature*, 404(6780):841–847, 2000.
- [12] Anthony J Bell and Terrence J Sejnowski. An information-maximization approach to blind separation and blind deconvolution. *Neural Computation*, 7(6):1129–1159, 1995.
- [13] Shun-Ichi Amari, Andrzej Cichocki, and Howard Yang. A new learning algorithm for blind signal separation. *Advances in Neural Information Processing Systems*, 8:757–763, 1995.
- [14] Dinh Tuan Pham and Philippe Garat. Blind separation of mixture of independent sources through a maximum likelihood approach. In *In proc. eusipco*. Citeseer, 1997.
- [15] Te-Won Lee. Independent component analysis. In *Independent component analysis*, pages 27–66. Springer, 1998.
- [16] Te-Won Lee, Mark Girolami, Anthony J Bell, and Terrence J Sejnowski. A unifying information-theoretic framework for independent component analysis. *Computers & Mathematics with Applications*, 39(11):1–21, 2000.
- [17] Juha Karhunen, Erkki Oja, Liuyue Wang, Ricardo Vigario, and Jyrki Joutsensalo. A class of neural networks for independent component analysis. *IEEE Transactions on Neural Networks*, 8(3):486–504, 1997.
- [18] Shun-Ichi Amari and Andrzej Cichocki. Adaptive blind signal processing-neural network approaches. *Proceedings of the IEEE*, 86(10):2026–2048, 1998.
- [19] Aapo Hyvärinen and Erkki Oja. Independent component analysis by general nonlinear Hebbian-like learning rules. *Signal Processing*, 64(3):301–313, 1998.

- [20] Andrzej Cichocki, Juha Karhunen, Włodzimierz Kasprzak, and Ricardo Vigarío. Neural networks for blind separation with unknown number of sources. *Neurocomputing*, 24(1-3):55–93, 1999.
- [21] Peter Földiák. Forming sparse representations by local anti-Hebbian learning. *Biological Cybernetics*, 64(2):165–170, 1990.
- [22] Ralph Linsker. A local learning rule that enables information maximization for arbitrary input distributions. *Neural Computation*, 9(8):1661–1665, 1997.
- [23] Cengiz Pehlevan, Sreyas Mohan, and Dmitri B Chklovskii. Blind nonnegative source separation using biological neural networks. *Neural Computation*, 29(11):2925–2954, 2017.
- [24] David Lipshutz and Dmitri B Chklovskii. Bio-NICA: A biologically inspired single-layer network for nonnegative independent component analysis. *arXiv preprint arXiv:2010.12632*, 2020.
- [25] Berfin Simsek and Alper T Erdogan. Online bounded component analysis: A simple recurrent neural network with local update rule for unsupervised separation of dependent and independent sources. In *2019 53rd Asilomar Conference on Signals, Systems, and Computers*, pages 1639–1643. IEEE, 2019.
- [26] Alper T Erdogan and Cengiz Pehlevan. Blind bounded source separation using neural networks with local learning rules. In *ICASSP 2020-2020 IEEE International Conference on Acoustics, Speech and Signal Processing (ICASSP)*, pages 3812–3816. IEEE, 2020.
- [27] J-F Cardoso. Source separation using higher order moments. In *ICASSP*, pages 2109–2112. IEEE, 1989.
- [28] Jari Miettinen, Sara Taskinen, Klaus Nordhausen, and Hannu Oja. Fourth moments and independent component analysis. *Statistical Science*, 30(3):372–390, 2015.
- [29] Tatsuya Hayama, Jun Noguchi, Satoshi Watanabe, Noriko Takahashi, Akiko Hayashi-Takagi, Graham CR Ellis-Davies, Masanori Matsuzaki, and Haruo Kasai. GABA promotes the competitive selection of dendritic spines by controlling local  $Ca^{2+}$  signaling. *Nature neuroscience*, 16(10):1409, 2013.
- [30] John NJ Reynolds, Brian I Hyland, and Jeffery R Wickens. A cellular mechanism of reward-related learning. *Nature*, 413(6851):67–70, 2001.
- [31] Humberto Salgado, Georg Köhr, and Mario Trevino. Noradrenergic ‘tone’ determines dichotomous control of cortical spike-timing-dependent plasticity. *Scientific reports*, 2(1):1–7, 2012.
- [32] Christian Henneberger, Thomas Papouin, Stéphane HR Oliet, and Dmitri A Rusakov. Long-term potentiation depends on release of d-serine from astrocytes. *Nature*, 463(7278):232–236, 2010.
- [33] OJMD Coenen, DM Eagleman, V Mitsner, TM Bartol, AJ Bell, and TJ Sejnowski. Cerebellar glomeruli: Does limited extracellular calcium direct a new kind of plasticity. In *Society for Neuroscience Abstracts*, volume 27, 2001.
- [34] Matti Weckström and Simon Laughlin. Extracellular potentials modify the transfer of information at photoreceptor output synapses in the blowfly compound eye. *Journal of Neuroscience*, 30(28):9557–9566, 2010.
- [35] Emily P Huang. Synaptic plasticity: a role for nitric oxide in LTP. *Current Biology*, 7(3):R141–R143, 1997.
- [36] Christian Hölscher. Nitric oxide, the enigmatic neuronal messenger: its role in synaptic plasticity. *Trends in neurosciences*, 20(7):298–303, 1997.
- [37] Neil Hardingham, James Dachtler, and Kevin Fox. The role of nitric oxide in pre-synaptic plasticity and homeostasis. *Frontiers in cellular neuroscience*, 7:190, 2013.
- [38] Karl Pearson. On lines and planes of closest fit to systems of points in space. *The London, Edinburgh, and Dublin Philosophical Magazine and Journal of Science*, 2(11):559–572, 1901.
- [39] Ian T Jolliffe. *Principal Component Analysis and Factor Analysis*, volume 1. Springer, 1986.
- [40] Kun Zhang and Lai-Wan Chan. ICA by PCA approach: relating higher-order statistics to second-order moments. In *International Conference on Independent Component Analysis and Signal Separation*, pages 311–318. Springer, 2006.

- [41] Erkki Oja. Principal components, minor components, and linear neural networks. *Neural Networks*, 5(6):927–935, 1992.
- [42] A-J Van Der Veen, ED F Depretere, and A Lee Swindlehurst. Subspace-based signal analysis using singular value decomposition. *Proceedings of the IEEE*, 81(9):1277–1308, 1993.
- [43] Cengiz Pehlevan and Dmitri Chklovskii. A normative theory of adaptive dimensionality reduction in neural networks. In *Advances in Neural Information Processing Systems*, pages 2269–2277, 2015.
- [44] Cengiz Pehlevan, Anirvan M Sengupta, and Dmitri B Chklovskii. Why do similarity matching objectives lead to Hebbian/anti-Hebbian networks? *Neural Computation*, 30(1):84–124, 2017.
- [45] Victor Minden, Cengiz Pehlevan, and Dmitri B Chklovskii. Biologically plausible online principal component analysis without recurrent neural dynamics. In *2018 52nd Asilomar Conference on Signals, Systems, and Computers*, pages 104–111. IEEE, 2018.
- [46] Cengiz Pehlevan and Dmitri B Chklovskii. A Hebbian/anti-Hebbian network derived from online non-negative matrix factorization can cluster and discover sparse features. In *2014 48th Asilomar Conference on Signals, Systems and Computers*, pages 769–775. IEEE, 2014.
- [47] Yanis Bahroun, Eugénie Hunsicker, and Andrea Soltoggio. Neural networks for efficient nonlinear online clustering. In *International Conference on Neural Information Processing*, pages 316–324. Springer, 2017.
- [48] Anirvan Sengupta, Cengiz Pehlevan, Mariano Tepper, Alexander Genkin, and Dmitri Chklovskii. Manifold-tiling localized receptive fields are optimal in similarity-preserving neural networks. In *Advances in Neural Information Processing Systems*, volume 31, 2018.
- [49] Yanis Bahroun, Dmitri Chklovskii, and Anirvan Sengupta. A similarity-preserving network trained on transformed images recapitulates salient features of the fly motion detection circuit. In *Advances in Neural Information Processing Systems*, volume 32, 2019.
- [50] Cengiz Pehlevan, Xinyuan Zhao, Anirvan M Sengupta, and Dmitri Chklovskii. Neurons as canonical correlation analyzers. *Frontiers in Computational Neuroscience*, 14:55, 2020.
- [51] David Lipshutz, Yanis Bahroun, Siavash Golkar, Anirvan M Sengupta, and Dmitri B Chklovskii. A biologically plausible neural network for multichannel canonical correlation analysis. *Neural Computation*, 33(9):2309–2352, 2021.
- [52] Yanis Bahroun and Andrea Soltoggio. Online representation learning with single and multi-layer Hebbian networks for image classification. In *International Conference on Artificial Neural Networks*, pages 354–363. Springer, 2017.
- [53] Shanshan Qin, Nayantara Mudur, and Cengiz Pehlevan. Contrastive similarity matching for supervised learning. *Neural Computation*, 33(5):1300–1328, 2021.
- [54] Yanis Bahroun and Dmitri B Chklovskii. A neural network with local learning rules for minor subspace analysis. *arXiv preprint arXiv:2102.05501*, 2021.
- [55] Kantilal V Mardia, John T Kent, and John M Bibby. *Multivariate Analysis (probability and mathematical statistics)*. Academic Press London, 1980.
- [56] Paul F Pinsky and John Rinzel. Intrinsic and network rhythmogenesis in a reduced Traub model for CA3 neurons. *Journal of computational neuroscience*, 1(1):39–60, 1994.
- [57] Sonia Gasparini and Jeffrey C Magee. State-dependent dendritic computation in hippocampal CA1 pyramidal neurons. *Journal of Neuroscience*, 26(7):2088–2100, 2006.
- [58] Nelson Spruston. Pyramidal neurons: dendritic structure and synaptic integration. *Nature Reviews Neuroscience*, 9(3):206–221, 2008.
- [59] Yael Katz, Vilas Menon, Daniel A Nicholson, Yuri Geinisman, William L Kath, and Nelson Spruston. Synapse distribution suggests a two-stage model of dendritic integration in CA1 pyramidal neurons. *Neuron*, 63(2):171–177, 2009.
- [60] Jordan Guerguiev, Timothy P Lillicrap, and Blake A Richards. Towards deep learning with segregated dendrites. *Elife*, 6:e22901, 2017.
- [61] João Sacramento, Rui Ponte Costa, Yoshua Bengio, and Walter Senn. Dendritic cortical microcircuits approximate the backpropagation algorithm. *Advances in Neural Information Processing Systems*, 31:8721–8732, 2018.

- [62] Blake A Richards and Timothy P Lillicrap. Dendritic solutions to the credit assignment problem. *Current opinion in neurobiology*, 54:28–36, 2019.
- [63] Siavash Golkar, David Lipshutz, Yanis Bahroun, Anirvan Sengupta, and Dmitri Chklovskii. A simple normative network approximates local non-hebbian learning in the cortex. *Advances in Neural Information Processing Systems*, 33, 2020.
- [64] Spyridon Chavlis and Panayiota Poirazi. Drawing inspiration from biological dendrites to empower artificial neural networks. *Current Opinion in Neurobiology*, 70:1–10, 2021.
- [65] Vincent Paille, Elodie Fino, Kai Du, Teresa Morera-Herreras, Sylvie Perez, Jeanette Hellgren Kotaleski, and Laurent Venance. GABAergic circuits control spike-timing-dependent plasticity. *Journal of Neuroscience*, 33(22):9353–9363, 2013.
- [66] Ji-Chuan Zhang, Pak-Ming Lau, and Guo-Qiang Bi. Gain in sensitivity and loss in temporal contrast of stdp by dopaminergic modulation at hippocampal synapses. *Proceedings of the National Academy of Sciences*, 106(31):13028–13033, 2009.
- [67] Sho Yagishita, Akiko Hayashi-Takagi, Graham CR Ellis-Davies, Hidetoshi Urakubo, Shin Ishii, and Haruo Kasai. A critical time window for dopamine actions on the structural plasticity of dendritic spines. *Science*, 345(6204):1616–1620, 2014.
- [68] Joshua P Johansen, Lorenzo Diaz-Mataix, Hiroki Hamanaka, Takaaki Ozawa, Edgar Ycu, Jenny Koivumaa, Ashwani Kumar, Mian Hou, Karl Deisseroth, Edward S Boyden, et al. Hebbian and neuromodulatory mechanisms interact to trigger associative memory formation. *Proceedings of the National Academy of Sciences*, 111(51):E5584–E5592, 2014.
- [69] Takuya Isomura and Taro Toyoizumi. A local learning rule for independent component analysis. *Scientific Reports*, 6(1):1–17, 2016.
- [70] Takuya Isomura and Taro Toyoizumi. Error-gated Hebbian rule: A local learning rule for principal and independent component analysis. *Scientific Reports*, 8(1):1–11, 2018.
- [71] Richard S Sutton. Learning to predict by the methods of temporal differences. *Machine learning*, 3(1):9–44, 1988.
- [72] Pietro Mazzoni, Richard A Andersen, and Michael I Jordan. A more biologically plausible learning rule for neural networks. *Proceedings of the National Academy of Sciences*, 88(10):4433–4437, 1991.
- [73] Ronald J Williams. Simple statistical gradient-following algorithms for connectionist reinforcement learning. *Machine learning*, 8(3-4):229–256, 1992.
- [74] Lukasz Kuśmierz, Takuya Isomura, and Taro Toyoizumi. Learning with three factors: modulating Hebbian plasticity with errors. *Current Opinion in Neurobiology*, 46:170–177, 2017.
- [75] Elie L Bienenstock, Leon N Cooper, and Paul W Munro. Theory for the development of neuron selectivity: orientation specificity and binocular interaction in visual cortex. *Journal of Neuroscience*, 2(1):32–48, 1982.
- [76] Erkki Oja. The nonlinear PCA learning rule in independent component analysis. *Neurocomputing*, 17(1):25–45, 1997.
- [77] Cengiz Pehlevan and Dmitri B Chklovskii. Neuroscience-inspired online unsupervised learning algorithms: Artificial neural networks. *IEEE Signal Processing Magazine*, 36(6):88–96, 2019.
- [78] Bruno A Olshausen and David J Field. Emergence of simple-cell receptive field properties by learning a sparse code for natural images. *Nature*, 381(6583):607–609, 1996.
- [79] Nathan Intrator and Leon N Cooper. Objective function formulation of the bcm theory of visual cortical plasticity: Statistical connections, stability conditions. *Neural Networks*, 5(1):3–17, 1992.
- [80] GC Castellani, N Intrator, H Shouval, and LN Cooper. Solutions of the bcm learning rule in a network of lateral interacting nonlinear neurons. *Network: Computation in Neural Systems*, 10(2):111–121, 1999.
- [81] Michiel Coesmans, John T Weber, Chris I De Zeeuw, and Christian Hansel. Bidirectional parallel fiber plasticity in the cerebellum under climbing fiber control. *Neuron*, 44(4):691–700, 2004.
- [82] Henrik Jörntell and Christian Hansel. Synaptic memories upside down: bidirectional plasticity at cerebellar parallel fiber-purkinje cell synapses. *Neuron*, 52(2):227–238, 2006.

- [83] Kaspar E Vogt and Marco Canepari. On the induction of postsynaptic granule cell–Purkinje neuron LTP and LTD. *The Cerebellum*, 9(3):284–290, 2010.
- [84] Lucas Parra and Paul Sajda. Blind source separation via generalized eigenvalue decomposition. *Journal of Machine Learning Research*, 4:1261–1269, 2003.
- [85] Christian Jutten and Jeanny Herault. Blind separation of sources, part i: An adaptive algorithm based on neuromimetic architecture. *Signal processing*, 24(1):1–10, 1991.
- [86] Beate Laheld and Jean-Francois Cardoso. Adaptive source separation with uniform performance. In *Proc. EUSIPCO*, volume 1, pages 183–186. Citeseer, 1994.
- [87] J-F Cardoso and Beate H Laheld. Equivariant adaptive source separation. *IEEE Transactions on signal processing*, 44(12):3017–3030, 1996.
- [88] Juha Karhunen, Liuyue Wang, and Ricardo Vigarío. Nonlinear pca type approaches for source separation and independent component analysis. In *Proceedings of ICNN’95-International Conference on Neural Networks*, volume 2, pages 995–1000. IEEE, 1995.
- [89] Peter Kabal. TSP speech database. *McGill University, Database Version*, 1(0):09–02, 2002.
- [90] Philemon Brakel and Yoshua Bengio. Learning independent features with adversarial nets for non-linear ICA. *arXiv preprint arXiv:1710.05050*, 2017.
- [91] Aapo Hyvärinen and Patrik Hoyer. Emergence of phase-and shift-invariant features by decomposition of natural images into independent feature subspaces. *Neural computation*, 12(7):1705–1720, 2000.
- [92] Jussi H Poikonen and Mika Laiho. Online linear subspace learning in an analog array computing architecture. In *CNNA 2016; 15th International Workshop on Cellular Nanoscale Networks and their Applications*, pages 1–2. VDE, 2016.
- [93] Mohammed E Fouda, Emre Neftci, Ahmed Eltawil, and Fadi Kurdahi. Independent component analysis using RRAMs. *IEEE Transactions on Nanotechnology*, 18:611–615, 2018.
- [94] Cengiz Pehlevan. A spiking neural network with local learning rules derived from nonnegative similarity matching. In *ICASSP 2019-2019 IEEE International Conference on Acoustics, Speech and Signal Processing (ICASSP)*, pages 7958–7962. IEEE, 2019.
- [95] J. D. Carroll. Generalization of canonical correlation analysis to three or more sets of variables. *Proc. APA*, pages 227–228, 1968.
- [96] David R Hardoon, Sandor Szedmak, and John Shawe-Taylor. Canonical correlation analysis: An overview with application to learning methods. *Neural Computation*, 16(12):2639–2664, 2004.
- [97] Lucas C. Parra. Multiset canonical correlation analysis simply explained. *arXiv preprint arXiv:1802.03759*, 2018.
- [98] Laurenz Wiskott and Terrence J Sejnowski. Slow feature analysis: Unsupervised learning of invariances. *Neural Computation*, 14(4):715–770, 2002.
- [99] Joel Zylberberg, Jason Timothy Murphy, and Michael Robert DeWeese. A sparse coding model with synaptically local plasticity and spiking neurons can account for the diverse shapes of V1 simple cell receptive fields. *PLoS computational biology*, 7(10):e1002250, 2011.
- [100] Paul D King, Joel Zylberberg, and Michael R DeWeese. Inhibitory interneurons decorrelate excitatory cells to drive sparse code formation in a spiking model of V1. *Journal of Neuroscience*, 33(13):5475–5485, 2013.
- [101] Sophie Denève, Alireza Alemi, and Ralph Bourdoukan. The brain as an efficient and robust adaptive learner. *Neuron*, 94(5):969–977, 2017.
- [102] Wieland Brendel, Ralph Bourdoukan, Pietro Vertech, Christian K Machens, and Sophie Denève. Learning to represent signals spike by spike. *PLoS computational biology*, 16(3):e1007692, 2020.
- [103] David Lipshutz, Charles Windolf, Siavash Golkar, and Dmitri Chklovskii. A biologically plausible neural network for slow feature analysis. In *Advances in Neural Information Processing Systems*, volume 33, pages 14986–14996, 2020.
- [104] James V Stone. Blind source separation using temporal predictability. *Neural Computation*, 13(7):1559–1574, 2001.

- [105] Hailin Liu and Yiuming Cheung. A learning framework for blind source separation using generalized eigenvalues. In *International Symposium on Neural Networks*, pages 472–477. Springer, 2005.
- [106] Tobias Blaschke, Pietro Berkes, and Laurenz Wiskott. What is the relation between slow feature analysis and independent component analysis? *Neural Computation*, 18(10):2495–2508, 2006.
- [107] Claudia Clopath, André Longtin, and Wulfram Gerstner. An online Hebbian learning rule that performs independent component analysis. In J. Platt, D. Koller, Y. Singer, and S. Roweis, editors, *Advances in Neural Information Processing Systems*, volume 20. Curran Associates, Inc., 2008.
- [108] Francis R Bach and Michael I Jordan. Kernel independent component analysis. *Journal of Machine Learning Research*, 3(Jul):1–48, 2002.
- [109] Yi-Ou Li, Tülay Adalı, Wei Wang, and Vince D Calhoun. Joint blind source separation by multiset canonical correlation analysis. *IEEE Transactions on Signal Processing*, 57(10):3918–3929, 2009.
- [110] Jean-Francois Cardoso and Antoine Souloumiac. Blind beamforming for non-Gaussian signals. *IEE Proceedings F (Radar and Signal Processing)*, 140(6):362–370, 1993.
- [111] Hannu Oja, Seija Sirkkiä, and Jan Eriksson. Scatter matrices and independent component analysis. *Austrian Journal of Statistics*, 35(2&3):175–189, 2006.
- [112] Esa Ollila, Hannu Oja, and Visa Koivunen. Complex-valued ICA based on a pair of generalized covariance matrices. *Computational Statistics & Data Analysis*, 52(7):3789–3805, 2008.
- [113] Ch Ziegauß and Elmar Wolfgang Lang. A neural implementation of the JADE algorithm (nJADE) using higher-order neurons. *Neurocomputing*, 56:79–100, 2004.
- [114] Aapo Hyvarinen, Hiroaki Sasaki, and Richard Turner. Nonlinear ICA using auxiliary variables and generalized contrastive learning. In *The 22nd International Conference on Artificial Intelligence and Statistics*, pages 859–868. PMLR, 2019.
- [115] Ilyes Khemakhem, Diederik Kingma, Ricardo Monti, and Aapo Hyvarinen. Variational autoencoders and nonlinear ICA: A unifying framework. In *International Conference on Artificial Intelligence and Statistics*, pages 2207–2217. PMLR, 2020.
- [116] Alexandre Payeur, Jordan Guerguiev, Friedemann Zenke, Blake A Richards, and Richard Naud. Burst-dependent synaptic plasticity can coordinate learning in hierarchical circuits. *Nature neuroscience*, pages 1–10, 2021.
- [117] Daniel D Lee and H Sebastian Seung. Learning the parts of objects by non-negative matrix factorization. *Nature*, 401(6755):788–791, 1999.
- [118] Cengiz Pehlevan et al. A Hebbian/anti-Hebbian neural network for linear subspace learning: A derivation from multidimensional scaling of streaming data. *Neural Computation*, 2015.
- [119] Christopher KI Williams. On a connection between kernel pca and metric multidimensional scaling. In *Advances in neural information processing systems*, pages 675–681, 2001.
- [120] Trevor F Cox and Michael AA Cox. *Multidimensional scaling*. CRC press, 2000.



## Supplementary Materials

This is the supplementary material for the NeurIPS titled ‘‘A Normative and Biologically Plausible Algorithm for Independent Component Analysis’’, from Yanis Bahroun, Dmitri B. Chklovskii, and Anirvan M. Sengupta.

### A Proof of our main theorem

We start by restating the setup in which our algorithm operates. The type of ICA considered in our work assumes the following generative model. There are  $d$  sources recorded  $T$  times forming the columns of  $\mathbf{S} := [\mathbf{s}_1, \dots, \mathbf{s}_T] \in \mathbb{R}^{d \times T}$  whose components  $s_t^1, \dots, s_t^d$  are assumed non-Gaussian and independent. Without loss of generality, we assume that each source has zero-mean, unit variance, and finite and distinct kurtosis, a common assumption among kurtosis-based ICA methods [28]. The kurtosis of a random variable  $v$  is defined as  $\text{kurt}[v] = \mathbb{E}[(v - \mathbb{E}(v))^4] / (\mathbb{E}[(v - \mathbb{E}(v))^2])^2$ . Finally, sources are assumed to be mixed through a linear system, i.e., there exists a full rank mixing matrix,  $\mathbf{A} \in \mathbb{R}^{d \times d}$ , producing the  $d$ -dimensional mixture,  $\mathbf{x}_t$ , expressed as

$$\mathbf{x}_t = \mathbf{A}\mathbf{s}_t \quad \forall t \in \{1, \dots, T\} . \quad (\text{S.1})$$

The goal of ICA algorithms is then to determine a signal,  $\mathbf{y}_t$ , obtained from a fixed linear transformation of the observed signal,  $\mathbf{x}_t$ , i.e.,  $\exists \mathbf{W}_{ICA} \in \mathbb{R}^{d \times d}$ , such that

$$\mathbf{y}_t = \mathbf{\Xi}\mathbf{\Pi}\mathbf{s}_t \quad \text{and} \quad \mathbf{y}_t := \mathbf{W}_{ICA}\mathbf{x}_t, \quad \forall t \in \{1, \dots, T\} , \quad (\text{S.2})$$

where  $\mathbf{\Xi}$  is a diagonal matrix with  $\pm 1$ 's on the diagonal, and  $\mathbf{\Pi}$  a permutation matrix. As a result,  $\mathbf{y}_t$  represents the ideally recovered unknown sources.

We now recall our objective function for ICA

$$\min_{\substack{\mathbf{Y} \in \mathbb{R}^{d \times T} \\ \frac{1}{T}\mathbf{Y}\mathbf{Y}^\top = \mathbf{I}_d}} \left\| \mathbf{X}^\top \mathbf{C}_x^{-1/2} \left[ \frac{1}{T} \sum_{t=1}^T \|\mathbf{C}_x^{-1/2}\mathbf{x}_t\|^2 \mathbf{C}_x^{-1/2}\mathbf{x}_t\mathbf{x}_t^\top \mathbf{C}_x^{-1/2} \right]^{-1} \mathbf{C}_x^{-1/2}\mathbf{X} - \mathbf{Y}^\top \mathbf{\Lambda}^2 \mathbf{Y} \right\|_F^2 . \quad (\text{S.3})$$

and finally our main theorem which is proved in the following.

**Theorem 2.** *Given that the sources are independent, centered, have unit variance, and distinct kurtosis (c.f. Sec 2 of the main text), then the global optimal solution for our objective (S.3), denoted by  $\mathbf{Y}^*$  satisfies*

$$\mathbf{Y}^* = \mathbf{\Xi}\mathbf{\Pi}\mathbf{S} \quad (\text{S.4})$$

where  $\mathbf{\Xi}$  and  $\mathbf{\Pi}$ , defined in (S.2), represents the sign and permutation ambiguity of the solution, and is thus a solution to the ICA problem.

We propose an outline of the proof.

- Proof of the FOBI procedure
- Proof that  $\mathbf{C}_z$  and  $\mathbf{C}_z^{-1}$  lead to the same solution of the eigenvalue problem solving FOBI.
- Note that  $\mathbf{C}_z^{-1}$  and  $\mathbf{C}_z^{-1/2}\mathbf{C}_h\mathbf{C}_z^{-1/2}$  are equivalent by whitening properties.
- Identify the Gramian associated with  $\mathbf{C}_z^{-1/2}\mathbf{C}_h\mathbf{C}_z^{-1/2}$ , which is  $\mathbf{H}^\top \mathbf{C}_z^{-1}\mathbf{H}$ .
- Use the Similarity matching formulation of principal component analysis on the aforementioned Gramian to finalize the proof.

#### A.1 Statements and Proofs of FIBO

We redefine important notations, i.e., the whitened data denoted by  $\mathbf{h}_t$  is defined as

$$\mathbf{h}_t = \mathbf{C}_x^{-1/2}\mathbf{x}_t .$$

Now the weighted whitened data, scaled by its norm, denoted by  $\mathbf{z}_t$ , is defined as

$$\mathbf{z}_t = \|\mathbf{h}_t\| \cdot \mathbf{h}_t .$$

We have defined the sample covariance matrix of  $\mathbf{x}_t$  and  $\mathbf{z}_t$  as  $\mathbf{C}_x$  and  $\mathbf{C}_z$  respectively.

Before, demonstrating our theorem, we need to demonstrate the main results of the FOBI procedure, i.e., we must show that when the whitened data,  $\mathbf{h}_t$  are projected onto the eigenvectors of the weighted data,  $\mathbf{z}_t$  they recover the sources. This results is stated and proved using the following theorem from [27, 40].

**Theorem 3.** *Let  $\mathbf{s}$ ,  $\mathbf{h}$ , and  $\mathbf{z}$  be random vectors such that  $\mathbf{h} = \mathbf{B}\mathbf{s}$ , where  $\mathbf{B}$  is an orthogonal matrix, and  $\mathbf{z} = \|\mathbf{h}\| \cdot \mathbf{h}$ . Suppose additionally  $\mathbf{s}$  has zero-mean independent components and these components have distinct finite kurtosis. Then the orthogonal matrix  $\mathbf{U}$  which gives the principal components of  $\mathbf{z}$  performs ICA on  $\mathbf{h}$ .*

*Proof.* Let  $\mathbf{s} = [s_1, \dots, s_d]^\top$ ,  $\mathbf{U} = [\mathbf{u}_1, \dots, \mathbf{u}_d]$ , and  $\mathbf{C} = [\mathbf{c}_1, \dots, \mathbf{c}_d] = [c_{ij}]_{d \times d} = \mathbf{U}\mathbf{B}$ . Since  $\mathbf{B}$  is orthogonal, we have  $\|\mathbf{h}\| = \|\mathbf{B}\mathbf{s}\| = \|\mathbf{s}\|$ . The second-order moment of the projection of  $\mathbf{z}$  on  $\mathbf{u}_i$  is

$$\begin{aligned} \mathbb{E}(\mathbf{u}_i^\top \mathbf{z})^2 &= \mathbb{E}(\mathbf{u}_i^\top \|\mathbf{h}\| \cdot \mathbf{h})^2 = \mathbb{E}(\|\mathbf{s}\|^2 \cdot (\mathbf{u}_i^\top \mathbf{B}\mathbf{s})^2) = \mathbb{E}\left(\sum_{k=1}^d (c_{ik}^\top \mathbf{s})^2 \cdot s_k^2\right) \\ &= \sum_{k=1}^d c_{ik}^2 \mathbb{E}(s_k^4) + \sum_{k=1}^d \sum_{p=1, p \neq k}^d c_{ip}^2 \mathbb{E}(s_p^2 s_k^2) + \sum_{k=1}^d \sum_{p=1, p \neq k}^d \sum_{q=1, q \neq p}^d c_{ip} c_{iq} \mathbb{E}(s_p s_q s_k^2) \end{aligned} \quad (\text{S.5})$$

When  $q \neq p$ , at least one of  $q$  and  $p$  is different from  $k$ . Suppose  $q \neq k$ . We then have  $\mathbb{E}(s_p s_q s_k^2) = \mathbb{E}(s_q) \mathbb{E}(s_p s_k^2) = 0$  since  $s_i$  are independent and zero-mean. We also have  $\sum_{k=1}^d c_{ik}^2 = 1$  since  $\mathbf{C}$  is orthogonal. Equation (S.5) then becomes

$$\begin{aligned} \mathbb{E}(\mathbf{u}_i^\top \mathbf{z})^2 &= \sum_{k=1}^d c_{ik}^2 \mathbb{E}(s_k^4) + \sum_{k=1}^d \sum_{p=1, p \neq k}^d c_{ip}^2 \mathbb{E}(s_p^2 s_k^2) \\ &= \sum_{k=1}^d c_{ik}^2 \mathbb{E}(s_k^4) + \sum_{k=1}^d \sum_{p=1, p \neq k}^d c_{ip}^2 \\ &= \sum_{k=1}^d c_{ik}^2 \text{kurt}(s_k) + d + 2 \end{aligned} \quad (\text{S.6})$$

Therefore  $\mathbb{E}(\mathbf{u}_i^\top \mathbf{z})^2$  is the weighted average of  $\text{kurt}(s_i)$  plus a constant. As  $s_i$  are assumed to have different kurtosis, without loss of generality, we assume  $\text{kurt}(s_1) > \text{kurt}(s_2) > \dots > \text{kurt}(s_n)$ . From Equation (S.6) we can see that maximization of  $\mathbb{E}(\mathbf{u}_1^\top \mathbf{z})^2$  gives  $\mathbf{c}_1 = [\pm 1, 0, \dots, 0]^\top$ , which means that  $y_1 = \mathbf{u}_1^\top \mathbf{h} = \mathbf{u}_1^\top \mathbf{B}\mathbf{s} = \mathbf{c}_1^\top \mathbf{s} = \pm s_1$ . After finding  $\mathbf{u}_1$ , under the constraint that  $\mathbf{u}_2$  is orthogonal to  $\mathbf{u}_1$ , the maximum of  $\mathbb{E}(\mathbf{u}_2^\top \mathbf{z})^2$  is obtained at  $\mathbf{c}_2 = [0, \pm 1, 0, \dots, 0]^\top$ . Consequently  $y_2 = \mathbf{u}_2^\top \mathbf{h} = \mathbf{c}_2^\top \mathbf{s} = \pm s_2$ . Repeating this procedure, finally all independent components can be estimated as  $y_i = \mathbf{u}_i^\top \mathbf{h} = \pm s_i$  where  $\mathbf{u}_i$  maximizes  $\mathbb{E}(\mathbf{u}_i^\top \mathbf{z})^2$ . In other words, the orthogonal matrix  $\mathbf{U}$  performing PCA on  $\mathbf{z}$  (without centering of  $\mathbf{z}$ ) actually performs ICA on  $\mathbf{h}$ .  $\square$

We have thus proved that the information about the eigenvectors of  $\mathbf{z}_t$  are enough for finding the sources after whitening.

## A.2 Eigenvalue Formulation

Now that we have clarified that the FOBI procedure consists of projecting the input data using Theorem 3, we can rephrase it as a generalized eigenvalue problem where  $\mathbf{W}$  is the solution of the following problem

$$\mathbf{W}\mathbf{W}^\top = \mathbf{I} \text{ and } \mathbf{W}\mathbf{C}_z\mathbf{W} = \mathbf{D} , \quad (\text{S.7})$$

with  $\mathbf{D}$  a diagonal matrix with distinct nonnegative diagonal elements. This problem is equivalent to

$$\tilde{\mathbf{W}}\tilde{\mathbf{W}}^\top = \mathbf{I} \ , \ \tilde{\mathbf{W}}\mathbf{C}_z^{-1}\tilde{\mathbf{W}}^\top = \mathbf{D}^{-1} \ , \quad (\text{S.8})$$

With  $\mathbf{H}$  and  $\mathbf{h}_t$ ,  $\mathbf{Z}$  and  $\mathbf{z}_t$  define as in the main text. This results from the fact that  $\mathbf{C}_z$  is assumed full rank and have distinct eigenvalue, the problem  $\mathbf{W}\mathbf{C}_z\mathbf{W} = \mathbf{D}$  has the same solution as  $\mathbf{W}\mathbf{C}_z^{-1}\mathbf{W} = \mathbf{D}^{-1}$  under orthogonality constraint.

Now we note that by definition  $\mathbf{C}_h = \frac{1}{T}\mathbf{H}\mathbf{H}^\top = \mathbf{I}_d$ , and that  $\mathbf{C}_z^{-1}$  is positive semi-definite thus admits a square-root. We can then rephrase the problem (S.8) as

$$\arg \max_{\hat{\mathbf{W}}^\top \hat{\mathbf{W}} = \mathbf{I}_d} \text{Tr}(\hat{\mathbf{W}}^\top \mathbf{C}_z^{-1/2} \mathbf{C}_h \mathbf{C}_z^{-1/2} \hat{\mathbf{W}}) = \arg \max_{\hat{\mathbf{W}}^\top \hat{\mathbf{W}} = \mathbf{I}_d} \text{Tr}(\hat{\mathbf{W}}^\top \mathbf{C}_z^{-1/2} \frac{1}{T} \mathbf{H}\mathbf{H}^\top \mathbf{C}_z^{-1/2} \hat{\mathbf{W}}) \quad (\text{S.9})$$

### A.3 From the covariance matrix to the Gram matrix

In the final step we need to consider the following matrix  $\mathbf{K} = \mathbf{H}\mathbf{C}_z^{-1/2}$ , which is a simple but essential rewriting of the eigenvalue problem (S.9) as

$$\arg \max_{\hat{\mathbf{W}}\hat{\mathbf{W}}^\top = \mathbf{I}_d} \text{Tr}(\hat{\mathbf{W}}\mathbf{K}\mathbf{K}^\top \hat{\mathbf{W}}^\top)$$

Now we rely on the result from Mardia et al.[55] for multidimensional scaling. Their results connects the eigenvalue and eigenvectors of the Gram matrix, i.e., matrix of similarity with that of the covariance matrix. This result was recently popularized by the similarity matching framework [43, 44] that states that the principal subspace projection can equivalently be obtained by

$$\arg \min_{\tilde{\mathbf{Y}}} \|\mathbf{K}^\top \mathbf{K} - \tilde{\mathbf{Y}}^\top \tilde{\mathbf{Y}}\|_F^2 = \arg \min_{\tilde{\mathbf{Y}}} \|\mathbf{H}^\top \mathbf{C}_z^{-1} \mathbf{H} - \tilde{\mathbf{Y}}^\top \tilde{\mathbf{Y}}\|_F^2$$

However this solution does the projection onto the principal subspace but does not recover the perfect sources as it is invariant by rotation which is a problem for ICA. Thus we include  $\mathbf{\Lambda}^2$  to break the symmetry as was done in [45]. The resulting objective function then leads to the same solution as the FOBI procedure.

$$\arg \min_{\substack{\mathbf{Y} \in \mathbb{R}^{d \times T} \\ \frac{1}{T} \mathbf{Y}\mathbf{Y}^\top = \mathbf{I}_d}} \|\mathbf{H}^\top \mathbf{C}_z^{-1} \mathbf{H} - \mathbf{Y}^\top \mathbf{\Lambda}^2 \mathbf{Y}\|_F^2$$

which is exactly our objective function (S.3)

$$\arg \min_{\substack{\mathbf{Y} \in \mathbb{R}^{d \times T} \\ \frac{1}{T} \mathbf{Y}\mathbf{Y}^\top = \mathbf{I}_d}} \left\| \mathbf{X}^\top \mathbf{C}_x^{-1/2} \left[ \frac{1}{T} \sum_{t=1}^T \|\mathbf{C}_x^{-1/2} \mathbf{x}_t\|^2 \mathbf{C}_x^{-1/2} \mathbf{x}_t \mathbf{x}_t^\top \mathbf{C}_x^{-1/2} \right]^{-1} \mathbf{C}_x^{-1/2} \mathbf{X} - \mathbf{Y}^\top \mathbf{\Lambda}^2 \mathbf{Y} \right\|_F^2 .$$

thus concluding the proof of Theorem 2.

## B Details of the illustrative example

We present the parameters used for our illustrative example for FOBI. We use a sinusoid waveform and a sawtooth signal as the independent sources. Each data source was then shuffled to remove possible temporal correlation, leading to fake dependence. We showed in Fig.1B 5000 datapoints. The mixing matrix  $\mathbf{A}$  was randomly chosen, and in the example is

$$\mathbf{A} = \begin{bmatrix} 0.10054428 & 0.81736508 \\ 0.75216771 & 0.44640104 \end{bmatrix}$$

It is then the observed data that are shown as  $\mathbf{x} = \mathbf{A}\mathbf{s}$ . The rest is described in the main text. The code used to produce the figure can be found attached to the submission, `NeurIPS_Fig_1A_procedure.ipynb`.

## C Numerics

### C.1 Detailed experimental figures

We propose zoomed in version of Fig.2B and 2C of the main showing respectively the speech separation and image separation tasks. We show in Fig. 3 the results obtained by our offline algorithm on the speech separation tasks as reported in the main text. We show in Fig. 4 the results obtained by our offline algorithm on the image separation tasks as reported in the main text. The codes used to produce the respective figures can be found attached to the submission, NeurIPS\_Fig\_2B\_audio, NeurIPS\_Fig\_2C\_image.

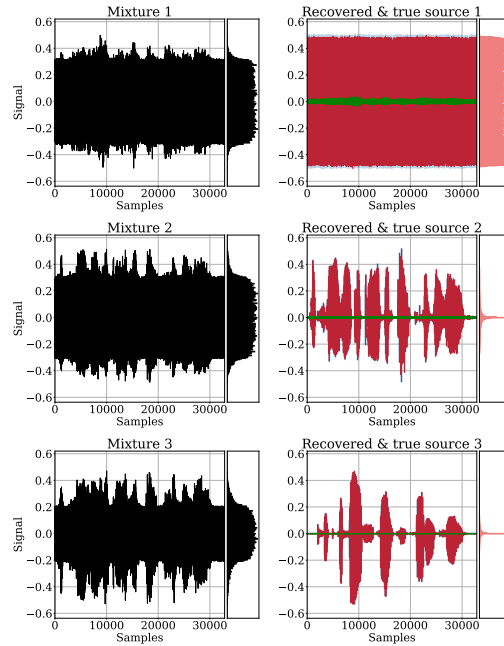


Figure 3: Illustration of the performance of our algorithm on the speech separation task. Our algorithm recovers the sources from mixed signals. It shows a zoomed in version of the results obtained for the speech separation task Fig.2.B of the main text. We show in black the mixed signals and in red (resp. blue) the recovered (resp. true) sources, and in green their difference called Residual. We also show the histogram of the associated distributions.

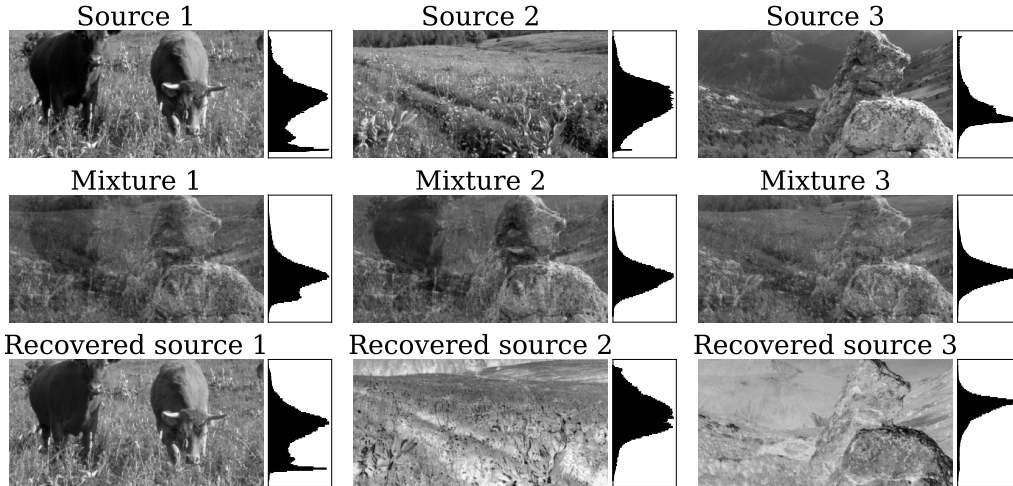


Figure 4: Illustration of the performance of our algorithm on the image separation task. Our algorithm recovers the sources from mixed images. It shows a zoomed in version of the results obtained for the image separation task Fig.2.C of the main text. We show in each row respectively the original sources, the mixed images, and the recovered along side their histograms.

## C.2 Online algorithm results

We show in Fig. 5 the results obtained by our online algorithm as defined in the main text. We also show in Fig. 6 the results obtained by our online algorithm on the image separation tasks as reported in the main text.

The results are almost identical to what we obtained in the offline case which confirms the relevance of our algorithm. Interestingly, in the speech separation task the noise is not entirely removed from one of the two voices which explains a “constant” value of the residual in green. However, for the image separation tasks the results are nearly identical.

The learning parameters are presented in the following subsection, and the codes used to produce the respective figures can be found attached to the submission, `NeurIPS_Fig_2B_audio`, `NeurIPS_Fig_2C_image`.

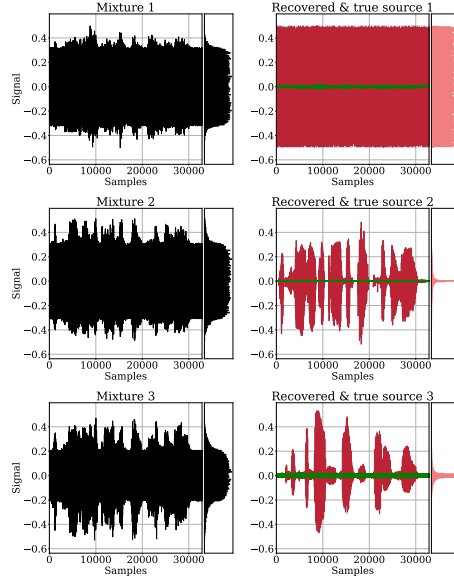


Figure 5: Performance of our online algorithm on the speech separation task. Our algorithm again recovers the sources from mixed signals. As was done for the offline version of our algorithm we show in black the mixed signals and in red (resp. blue) the recovered (resp. true) sources, and in green their difference called Residual. We also show the histogram of the associated distributions.

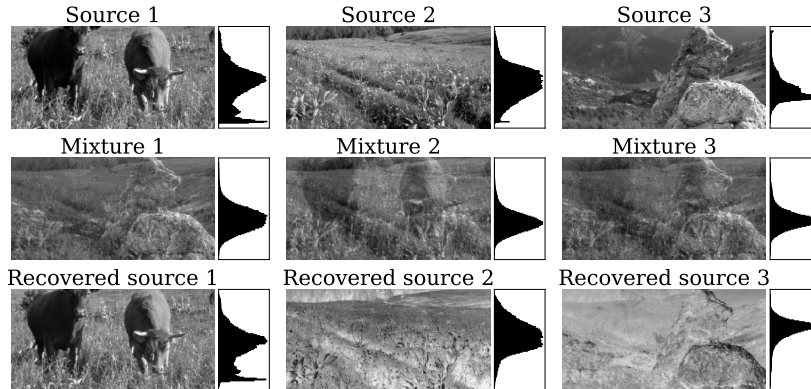


Figure 6: Performance of our online algorithm on the image separation task. Our algorithm again recovers the sources from mixed images. As was done for the offline algorithm we show in each row respectively the original sources, the mixed images, and the recovered alongside their histograms.

### C.3 Experimental details

We implemented both the offline and online version of our similarity-preserving algorithm, Algorithm 1 of the main text. We initialized  $\mathbf{W}$  to be a random matrix with i.i.d. mean-zero normal entries with variance 1. We initialized  $\mathbf{M}$  to be the identity matrix  $\mathbf{I}_d$ . We used fixed learning rates for  $\eta$  and  $\tau$ . The use of time-varying learning did not appear to change the results significantly and might instead lead to over-parameter tuning, which is arguably biologically implausible. We nonetheless performed grid-search to find the optimal hyperparameters, we performed a grid search over  $\eta_0 \in \{10^{-2}, 10^{-3}, 10^{-4}, 10^{-5}\}$ , each multiplied by 1, 2 or 5. For we used  $\tau \in \{2, 1.5, 1, 0.9, 0.85, 0.75, 0.5, 0.1\}$ . The best performing parameters are reported in Table 1. The results obtained with these parameters are presented in the main text, for Offline SM-ICA Fig.2A,2B and 2C. And the online SM-ICA Fig.3ABC below.

Algorithm	parameters	synthetic	audio	image
<b>Offline SM-ICA</b>	$\eta, \tau$	$5 \cdot 10^{-3}, 0.75$	$5 \cdot 10^{-4}, 0.85$	$5 \cdot 10^{-3}, 0.75$
	$\Lambda$	[1.0, 1.5, 1.8, 6.07]	[1.8, 6.15, 19.7]	[2.48, 3.06, 6.64]
<b>Online SM-ICA</b>	$\eta, \tau$	$2 \cdot 10^{-5}, 1.5$	$2 \cdot 10^{-5}, 1.5$	$2 \cdot 10^{-5}, 1.5$
	$\Lambda$	[1.0, 1.5, 1.8, 6.07]	[1.8, 6.15, 19.7]	[2.48, 3.06, 6.64]

Table 1: Training parameters for comparing our model.

## D Comparison to other models on the synthetic dataset

In this section, we compare numerically the performance of our algorithm against competing models on four different scenarios.

### D.1 Experimental details

**Metrics.** First of all we define the metric used to quantitatively compare the ICA algorithms. As defined in Sec. 2 of the main text, the task of ICA algorithms is to extract the source signals up to a permutation and sign-flipping (Eq. (2)). Therefore, all results are measured by considering all possible pairings of predicted signals and source signals, and measuring the mean-squared error  $\varepsilon_{\text{MSE}}$  defined as

$$\varepsilon_{\text{MSE}}(t) = \min_{\Xi, \mathbf{P}} \frac{1}{td} \sum_{t'=1}^t \|\mathbf{s}_{t'} - \Xi \mathbf{P} \mathbf{y}_{t'}\|^2 \quad (\text{S.10})$$

**Dataset.** We evaluate our algorithm on a synthetic dataset generated by independent and identically distributed samples. The data are generated from meaningful signals, i.e., square-periodic, sine-wave, saw-tooth, and Laplace random noise. The data were chosen with the purpose of including both super- and sub-Gaussian distribution known respectively as leptokurtic (“spiky”, e.g., the Laplace distribution) and platykurtic (“flat-topped”, the three other source signal).

**Scenarios.** We designed four scenarios: scenario 1, data are white and composed of 3 independent sub-Gaussian sources; scenario 2, data are colored and again composed of only 3 sub-Gaussian sources; scenario 3, data are white and composed of 2 sub-Gaussian sources and 1 super-Gaussian source; scenario 4, Data are colored and composed of 2 sub-Gaussian sources and 1 super-Gaussian source.

**Competing algorithms.** To quantitatively measure the performance we present in Appendix D a numerical comparison of our algorithm with competing algorithms, namely, Herault Jutten algorithm [85], EASI algorithm [86, 87], Bell and Sejnowski’s algorithm [12], the Amari algorithm [13], and finally nonlinear Oja algorithm [88, 76], on the synthetic data set, on three different scenarios. These models were designed with NNs in mind and are seminal works on neural ICA algorithms. However, like nonlinear Oja algorithm, which we mentioned in Section 5.3.1, these models suffer from biological implausibility.

Algo	param.	Scenario 1	Scenario 2	Scenario 3	Scenario 4
<b>Online SM-ICA (ours)</b>	$\eta, \tau$	$5 \cdot 10^{-3}, 0.75$	$5 \cdot 10^{-4}, 0.85$	$5 \cdot 10^{-3}, 0.75$	$5 \cdot 10^{-4}, 0.85$
	$\Lambda^{-1}$	[1.0, 1.5, 1.8]	[1.0, 1.5, 1.8]	[1.0, 1.5, 6.07]	[1.0, 1.5, 6.07]
<b>HJ</b> [85]	$\eta$	$10^{-4}$	$10^{-4}$	$10^{-4}$	$10^{-4}$
<b>EASI</b> [87]	$\eta$	$10^{-4}$	$10^{-4}$	$10^{-4}$	$10^{-4}$
<b>Nonlin. Oja</b> [76]	$\eta$	$10^{-3}$	$10^{-3}$	$10^{-3}$	$10^{-3}$
<b>Infomax</b> [12]	$\eta$	$5 \cdot 10^{-4}$	$5 \cdot 10^{-4}$	$5 \cdot 10^{-4}$	$5 \cdot 10^{-4}$
<b>Amari</b> [13]	$\eta$	$5 \cdot 10^{-4}$	$5 \cdot 10^{-4}$	$5 \cdot 10^{-4}$	$5 \cdot 10^{-4}$

Table 2: Training parameters of the different models on the four different scenarios.

## D.2 Results

We show in Fig. 7a the comparison between our model and competing algorithm on Scenario 1. Scenario 1 consists of a mixture of sub-Gaussian distribution, which has been pre-whitened. Naturally, in scenario 1, all models perform the task perfectly, with Nonlinear Oja and Amari algorithm being the fastest, our model also performs competitively.

We show in Fig. 7b the comparison between our model and competing algorithm on Scenario 2. Scenario 2 consists of a mixture of sub-Gaussian distribution, which has not been pre-whitened. In scenario 2, our algorithm is more competitive as it does not require pre-whitening, unlike the algorithms that fail at the task.

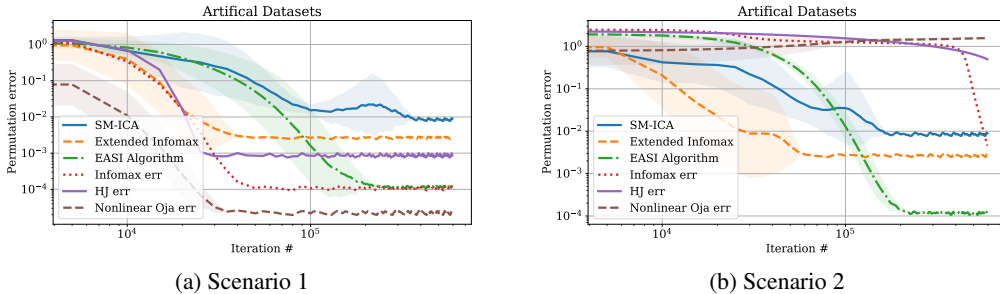


Figure 7: Comparison of the models on mixture of sub-Gaussian distribution, with (a) whitened data, and (b) colored data.

We show in Fig. 8a the comparison between our model and competing algorithm on Scenario 3. Scenario 3 consists of a mixture of both sub-Gaussian and super-Gaussian distribution, which has been pre-whitened. Again, our algorithm is more competitive as it has the ability to separate sources from a different sign of kurtosis, as explained in the main body of the paper.

We show in Fig. 8b the comparison between our model and competing algorithm on Scenario 4. Scenario 4 consists of a mixture of both sub-Gaussian and super-Gaussian distributions, which have not been pre-whitened. In this scenario, our algorithm performs one of the best as it does not require pre-whitening and can separate sources with a different sign of kurtosis.

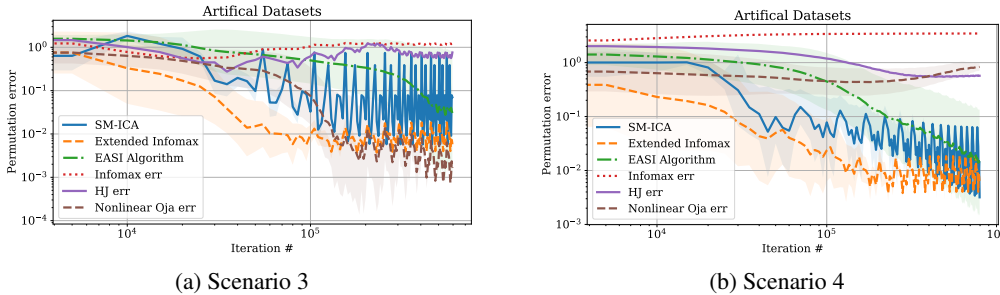


Figure 8: Comparison of the models on mixture of both sub- and super-Gaussian distribution, with (a) whitened data, and (b) colored data.

In brief, our model outperforms either outperforms or is competitive with other models on scenarios 2-3-4. Out of the other algorithms, EASI performs well on scenarios 1-2 but fails on tasks 3-4, where data are composed of both sub-Gaussian and super-Gaussian distributions. The other models are known to require pre-whitening and fail on scenarios 2 and 4, naturally. We have prepared a log-log plot of convergence with error bars that illustrate the results mentioned above. These results also confirm that our algorithm performs perfect separation with both whitened and colored data and simultaneously with both sub and super-Gaussian sources.



## E Contrasting reconstruction and similarity-preservation NNs

We mention in Section 2 and Section 5 of the paper that neural networks trained with Oja’s rule lack biological plausibility, unlike NNs resulting from the similarity matching framework. This statement can be unclear for people not too familiar with the approach. For that purpose, we recall the critical distinction between the similarity matching framework and the reconstruction-based approach from which Oja’s results. A more detailed description can be found in [77, 49].

To introduce our notation, the input to the NN is a set of vectors,  $\mathbf{x}_t \in \mathbb{R}^n, t = 1, \dots, T$ , with components represented by the activity of  $n$  upstream neurons at time,  $t$ . In response, the NN outputs an activity vector,  $\mathbf{y}_t \in \mathbb{R}^m, t = 1, \dots, T$ , where  $m$  is the number of output neurons.

**Reconstructive Approach:** The reconstruction approach starts with minimizing the squared reconstruction error:

$$\min_{\mathbf{W}, \mathbf{y}_{t=1 \dots T} \in \mathbb{R}^m} \sum_t \|\mathbf{x}_t - \mathbf{W}\mathbf{y}_t\|^2 = \min_{\mathbf{W}, \mathbf{y}_{t=1 \dots T} \in \mathbb{R}^m} \sum_{t=1}^T \left[ \|\mathbf{x}_t\|^2 - 2\mathbf{x}_t^\top \mathbf{W}\mathbf{y}_t + \mathbf{y}_t^\top \mathbf{W}^\top \mathbf{W}\mathbf{y}_t \right]. \quad (\text{S.11})$$

This objective is optimized offline by a projection onto the principal subspace of the input data.

In an online setting, the objective can be optimized by alternating minimization [78]. After the arrival of data sample,  $\mathbf{x}_t$ : firstly, the objective (S.11) is minimized with respect to the output,  $\mathbf{y}_t$ , while the weights,  $\mathbf{W}$ , are kept fixed, secondly, the weights are updated according to the following learning rule derived by a gradient descent with respect to  $\mathbf{W}$  for fixed  $\mathbf{y}_t$ :

$$\dot{\mathbf{y}}_t = \mathbf{W}_{t-1}^\top \mathbf{x}_t - \mathbf{W}_{t-1}^\top \mathbf{W}_{t-1} \mathbf{y}_t, \quad \mathbf{W}_t \leftarrow \mathbf{W}_{t-1} + \eta (\mathbf{x}_t - \mathbf{W}_{t-1} \mathbf{y}_t) \mathbf{y}_t^\top, \quad (\text{S.12})$$

In the NN implementations of the algorithm (S.12), the elements of matrix  $\mathbf{W}$  are represented by synaptic weights and principal components by the activities of output neurons  $y_j$ , Fig. 9a [41].

However, implementing update (S.12)right in the single-layer NN architecture, Fig. 9a, requires non-local learning rules making it biologically implausible. Indeed, the last term in (S.12)right implies that updating the weight of a synapse requires the knowledge of output activities of all other neurons which are not available to the synapse. Moreover, the matrix of lateral connection weights,  $-\mathbf{W}_{t-1}^\top \mathbf{W}_{t-1}$ , in the last term of (S.12)left is computed as a Gramian of feedforward weights; a non-local operation. This problem is not limited to PCA and arises in nonlinear NNs as well [78, 117].

**Similarity Matching Approach:** To address these difficulties, [118] derived NNs from similarity-preserving objectives, as presented in Section 3. Such objectives require that similar input pairs,  $\mathbf{x}_t$  and  $\mathbf{x}_{t'}$ , evoke similar output pairs,  $\mathbf{y}_t$  and  $\mathbf{y}_{t'}$ . If the similarity of a pair of vectors is quantified by their scalar product, one such objective is similarity matching (SM):

$$\min_{\forall t \in \{1, \dots, T\}: \mathbf{y}_t \in \mathbb{R}^m} \frac{1}{2} \sum_{t, t'=1}^T (\mathbf{x}_t \cdot \mathbf{x}_{t'} - \mathbf{y}_t \cdot \mathbf{y}_{t'})^2. \quad (\text{S.13})$$

This offline optimization problem is also solved by projecting the input data onto the principal subspace [119, 120, 55]. Remarkably, the optimization problem (S.13) can be converted algebraically to a tractable form by introducing variables  $\mathbf{W}$  and  $\mathbf{M}$  [44]:

$$\min_{\{\mathbf{y}_t \in \mathbb{R}^m\}_{t=1}^T} \min_{\mathbf{W} \in \mathbb{R}^{n \times m}} \max_{\mathbf{M} \in \mathbb{R}^{m \times m}} \left[ \sum_{t=1}^T (-2\mathbf{x}_t^\top \mathbf{W}\mathbf{y}_t + \mathbf{y}_t^\top \mathbf{M}\mathbf{y}_t) + T \text{Tr}(\mathbf{W}^\top \mathbf{W}) - \frac{T}{2} \text{Tr}(\mathbf{M}^\top \mathbf{M}) \right]. \quad (\text{S.14})$$

In the online setting, first, we minimize (S.14) with respect to the output variables,  $\mathbf{y}_t$ , by gradient descent while keeping  $\mathbf{W}$ ,  $\mathbf{M}$  fixed [118]:

$$\dot{\mathbf{y}}_t = \mathbf{W}^\top \mathbf{x}_t - \mathbf{M}\mathbf{y}_t. \quad (\text{S.15})$$

To find  $\mathbf{y}_t$  after presenting the corresponding input,  $\mathbf{x}_t$ , (S.15) is iterated until convergence. After the convergence of  $\mathbf{y}_t$ , we update  $\mathbf{W}$  and  $\mathbf{M}$  by gradient descent and gradient ascent respectively [118]:

$$W_{ij} \leftarrow W_{ij} + \eta (x_i y_j - W_{ij}), \quad M_{ij} \leftarrow M_{ij} + \eta (y_i y_j - M_{ij}). \quad (\text{S.16})$$

Algorithm (S.15), (S.16) can be implemented by a biologically plausible NN, Fig. 9b. As before, activity (firing rate) of the upstream neurons encodes input variables,  $\mathbf{x}_t$ . Output variables,  $\mathbf{y}_t$ , are computed by the dynamics of activity (S.15) in a single layer of neurons. The elements of matrices  $\mathbf{W}$  and  $\mathbf{M}$  are represented by the weights of synapses in feedforward and lateral connections respectively. The learning rules (S.16) are local, i.e. the weight update,  $\Delta W_{ij}$ , for the synapse between  $i^{\text{th}}$  input neuron and  $j^{\text{th}}$  output neuron depends only on the activities,  $x_i$ , of  $i^{\text{th}}$  input neuron and,  $y_j$ , of  $j^{\text{th}}$  output neuron, and the synaptic weight. Learning rules (S.16) for synaptic weights  $\mathbf{W}$  and  $-\mathbf{M}$  (here minus indicates inhibitory synapses, see Eq.(S.15)) are Hebbian and anti-Hebbian respectively.

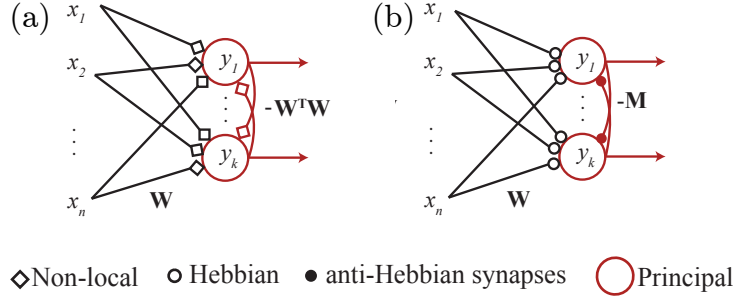


Figure 9: Single-layer NNs performing online (a) reconstruction error minimization (S.11) [41, 78], (b) similarity matching (SM) (S.13) [118].

**Comparison between the two approaches:** We now compare the objective functions of the two approaches. After dropping invariant terms, the reconstructive objective function has the following interactions among input and output variables:  $-2\mathbf{x}_t^T \mathbf{W} \mathbf{y}_t + \mathbf{y}_t^T \mathbf{W}^T \mathbf{W} \mathbf{y}_t$  (Eq S.11). The SM approach leads to  $-2\mathbf{x}_t^T \mathbf{W} \mathbf{y}_t + \mathbf{y}_t^T \mathbf{M} \mathbf{y}_t$ , (Eq S.14). The term linear in  $\mathbf{y}_t$ , a cross-term between inputs and outputs,  $-2\mathbf{x}_t^T \mathbf{W} \mathbf{y}_t$ , is common in both approaches and is responsible for projecting the data onto the principal subspace via the feedforward connections in Fig.1ab. The terms quadratic in  $\mathbf{y}_t$ 's decorrelate different output channels via a competition implemented by the lateral connections in Fig.1ab and are different in the two approaches. In particular, the inhibitory interaction between neuronal activities  $y_j$  in the reconstruction approach depends upon  $\mathbf{W}^T \mathbf{W}$ , which is tied to trained  $\mathbf{W}$  in a non-local way. In contrast, in the SM approach the inhibitory interaction matrix  $\mathbf{M}$  is learned for  $y_j$ 's via a local anti-Hebbian rule.

## F Paper Checklist

The checklist follows the references. Please read the checklist guidelines carefully for information on how to answer these questions. For each question, change the default **[TODO]** to **[Yes]**, **[No]**, or **[N/A]**. You are strongly encouraged to include a **justification to your answer**, either by referencing the appropriate section of your paper or providing a brief inline description. For example:

- Did you include the license to the code and datasets? **[Yes]** See Section 6
- Did you include the license to the code and datasets? **[No]** The code and the data will be made publicly available but for now are included with the submission.
- Did you include the license to the code and datasets? **[N/A]**

Please do not modify the questions and only use the provided macros for your answers. Note that the Checklist section does not count towards the page limit. In your paper, please delete this instructions block and only keep the Checklist section heading above along with the questions/answers below.

1. For all authors...
  - (a) Do the main claims made in the abstract and introduction accurately reflect the paper's contributions and scope? **[Yes]** Yes, we clearly state the setup in which we work, i.e., kurtosis-based linear ICA with sources with finite distinct kurtosis and search for a biologically plausible neural network.

- (b) Did you describe the limitations of your work? **[Yes]** Yes, we describe extensively the limitations of our model in Sec 7. We also mention possible future research direction
  - (c) Did you discuss any potential negative societal impacts of your work? **[N/A]** We do not foresee any negative impact rather positive one, it can have wide-ranging benefits for helping to manage the adverse effects of neurological disorders.
  - (d) Have you read the ethics review guidelines and ensured that your paper conforms to them? **[Yes]** Yes.
2. If you are including theoretical results...
- (a) Did you state the full set of assumptions of all theoretical results? **[Yes]** Yes.
  - (b) Did you include complete proofs of all theoretical results? **[Yes]** We left the proofs in the supplementary materials but gave some intuitions illustrated with toy examples as in Fig. 1B.
3. If you ran experiments...
- (a) Did you include the code, data, and instructions needed to reproduce the main experimental results (either in the supplemental material or as a URL)? **[Yes]** We include the code to the supplemental material.
  - (b) Did you specify all the training details (e.g., data splits, hyperparameters, how they were chosen)? **[Yes]** Yes, we explain how data are generated, and where the datasets used are available as well as training parameters.
  - (c) Did you report error bars (e.g., with respect to the random seed after running experiments multiple times)? **[Yes]** For Figs. in the supplementary material for comparison with existing non-biologically plausible models.
  - (d) Did you include the total amount of compute and the type of resources used (e.g., type of GPUs, internal cluster, or cloud provider)? **[Yes]** We only run on a basic computer as the model is online and is designed to not require much computing power and memory.
4. If you are using existing assets (e.g., code, data, models) or curating/releasing new assets...
- (a) If your work uses existing assets, did you cite the creators? **[Yes]** In Sec 6
  - (b) Did you mention the license of the assets? **[No]** All data used either synthetic data or publicly available.
  - (c) Did you include any new assets either in the supplemental material or as a URL? **[No]** No new assets aside from our code of the new algorithm.
  - (d) Did you discuss whether and how consent was obtained from people whose data you're using/curating? **[N/A]**
  - (e) Did you discuss whether the data you are using/curating contains personally identifiable information or offensive content? **[N/A]**
5. If you used crowdsourcing or conducted research with human subjects...
- (a) Did you include the full text of instructions given to participants and screenshots, if applicable? **[N/A]**
  - (b) Did you describe any potential participant risks, with links to Institutional Review Board (IRB) approvals, if applicable? **[N/A]**
  - (c) Did you include the estimated hourly wage paid to participants and the total amount spent on participant compensation? **[N/A]**